Modulation of NAD+/NADH Levels in ARPE-19 Cells Leads to Functional Changes in Oxidative Phosphorylation and Glycolysis

Modulation of NAD^+/NADH Levels in ARPE-19 Cells Leads to Functional Changes in Oxidative Phosphorylation and Glycolysis

Adrian Will-Orrego

A Thesis in the Field of Biotechnology

for the Degree of Master of Liberal Arts in Extension Studies

Harvard University

May 2020

Abstract

Dysregulation of the retinal pigmented epithelial cell (RPE) metabolism through mitochondrial dysfunction leads to photoreceptor degradation, implicating the RPE cell in retinal degeneration (Zhao et al., 2011). Aging decreases bioavailability of NAD^+ (Goody & Henry, 2018; Liu et al., 2012) , increasing likelihood of dysregulation in a host of NAD^+-regulated pathways, like the sirtuin family of proteins which regulate cellular metabolism, DNA repair, and other crucial functions (Avalos, Bever, & Wolberger, 2005; Gaur et al., 2017). NAMPT is the rate-limiting enzyme of the salvage pathway, responsible for recycling NAM and setting up NAD^+ biosynthesis. We hypothesize disruption of NAD^+ biosynthesis by inhibiting NAMPT will imbalance the NAD^+/NAM ratio and downregulate genes controlled by the Sirtuin family leading to functional changes in metabolism and cellular health.

Our experiments demonstrate intracellular levels of NAD^+/NADH are crucial to ARPE-19 cell function. Decreasing available NAD^+/NADH downregulates expression of genes associated with RPE activity and differentiation. Dysfunctional RPE cells generate less mitochondrial sourced ATP becoming heavily reliant on glycolysis for energy. Supplementing NAMPT inhibited ARPE-19 cells with NMN (a NAD precursor) reversed SeaHorse assay metabolic dysfunction phenotype and qPCR molecular signature potentially reverting ARPE-19 function to baseline. Further characterization of NAD^+/NADH dysregulation in human retina may yield insights into macular degeneration.

Acknowledgments

I would not have been able to complete this thesis without the help of my many peers, mentors, and collaborators who shaped me into the scientist I am today. I have been fortunate to learn from the best scientists in the field and for that I am thankful. First, to Dr. Jorge Aranda, my thesis director, for encouraging me to dig deeper and run more studies to get the complete picture. Dr. Aranda has been an exceptional mentor and manager, and I truly appreciate all his guidance and advice throughout the thesis process. It has been a mad dash, and I could not have completed it without your efforts.

To Dr. James Morris, my thesis adviser, for going the extra mile for me and ensuring that I got all my paperwork in time. This whole process would have been pushed back if it was not for your help, and I thank you.

To Shubh Dhillon and Megan Jabour who patiently taught me every tissue culture technique and assay I know, and for always being willing to answer my questions, troubleshoot problems, and look at images. This work could not have been done without your teachings, and I cannot thank you both enough.

To Barrett Leehy and Dr. Tony Walshe, the metabolism experts who made sure all of my extracellular flux assays were thorough and controlled perfectly. I would still be staring at the seahorse graphs if it was not for their wealth of experience and willingness to collaborate.

Table of Contents

List of Tables

List of Figures

Chapter I.

Introduction

Aging and Age-Related Macular Degeneration

Age-Related Macular Degeneration (AMD) is the leading causes of vision loss in the developed world (Jager, Mieler, & Miller, 2008; Lim, Mitchell, Seddon, Holz, & Wong, 2012). Early AMD is characterized by the accumulation of lipid deposits, *drusen*, which are clinically visible small yellow spots in the retina, located between the RPE and the choroidal vasculature. The presence of larger drusen and pigmentary changes in the RPE characterize intermediate and late-stage AMD. Drusen and pigment indicate an element of dysfunction in the photoreceptors and retinal pigment epithelium (RPE) and are associated with subjective loss of visual quality, especially in dim light conditions. (Balaratnasingam et al., 2016). In the advanced disease stages (geographic atrophy), photoreceptor and RPE cells progressively die in greater numbers, are removed by microglia cells (resident mononuclear phagocytes) potentially inducing bystander damage and progression of AMD pathology (Kauppinen, Paterno, Blasiak, Salminen, & Kaarniranta, 2016). Current treatments for AMD are only available for the neovascular (nv) or "wet" form of the disease. In wet AMD, pathological blood vessels grow into the RPE from the choroid in response to increased VEGF production from dysregulated RPE and activated microglia. Wet AMD only accounts for 10% of all cases, and requires regular intraocular injections of anti-VEGF therapy which improves vision by reducing leakage of fluid from the new blood vessels (angiogenesis). To date, there are no

approved treatments for the non-exudative/dry form of the disease (Prasad, Schwartz, & Hubschman, 2010) indicating a large unmet medical need.

The surviving photoreceptors and RPE at the geographic atrophy stage of AMD are highly dysregulated and many cells have already died, thus the likelihood of finding an effective treatment is low. By targeting therapies to earlier stages of AMD, delay or prevention of progression to the later stages of disease might be possible. A relevant *in vitro* or *in vivo* AMD model would be very helpful to develop candidate therapies. Modeling AMD *in vivo* is challenging. Rodents, for example, do not have a macula and have distinct immune systems and lipid metabolism processes from humans. AMD research frequently utilizes a spontaneously immortalized RPE cell line, the ARPE-19 cell.

The RPE cell is responsible for many key vision related processes (Figure 1). Primarily, the RPE recharges and recycles visual cycle proteins (retinoids) to photoreceptors enabling responses to photons of light. RPE cells transport glucose from the circulation to the photoreceptors and digest 10% of the total photoreceptor outer segment length each day (Kevany & Palczewski, 2010). Retinoid recycling and outer segment processing are very energy demanding processes. To support this high energy demand, the RPE is adjacent to the choriocapillaris, a highly vascular blood supply, enabling a steady supply of nutrients and oxygen. RPE dysfunction can lead to lipid accumulation on either the retinal (apical) or choroidal (basal) side of the RPE. This "lipid wall" prevents nutrient and visual cycle component transport, resulting in further visual dysfunction and photoreceptor cell stress (Curcio, 2018).

Dysregulation of RPE metabolism through mitochondrial dysfunction contributes to photoreceptor dysregulation, implicating the RPE cell as a source of retinal degeneration (Zhao et al., 2011). We aim to disrupt the metabolism of the RPE cell to recreate disease-like dysfunction. Aging has been associated with disruption of the NAD^+/NAM balance in multiple tissues (Moon & Minhas, 2017) and may be one of the earliest molecular changes associated with AMD. An RPE cell in a metabolic crisis would not perform the retinal homeostatic activities thus contributing to chronic damage to the photoreceptors and leading to loss of vision over time.

In vitro models may be able to identify pathways associated with AMD disruption of cellular metabolism in a disease-relevant cell line, or in response to disease-relevant stressors/insults.

Nicotinamide (NAM)

NAM, from the family of B3 vitamins, is essential for many cellular functions and is most commonly associated with incorporation into the coenzyme Nicotinamide Adenine Dinucleotide (NAD^+/NADH). Both NAM and NAD^+/NADH regulate multiple cellular pathways. Maintaining a proper NAD^+/NAM balance is integral to proper cell function (Figure 2). NAD^+ bioavailability is disrupted by aging (Goody & Henry, 2018; Liu et al., 2012) shifting the balance towards NAM, increasing the risk of dysregulation in a host of pathways. Ratios of NAM and NAD^+/NADH regulate sirtuins, a family of proteins responsible for many functions including maintaining proper mitochondrial function (Imai & Guarente, 2014), DNA repair (Jarrett & Boulton, 2007), and glycolysis (Imai & Guarente, 2014). The shift in the balance of NAD^+/NADH to NAM can lead to

lower mitochondrial activity (Figure 2), as reported in AMD patients (Feher et al., 2006). NAM accumulation can also disrupt the activity of sirtuin family members (Avalos et al., 2005; Guan, Lin, Knoll, & Chakrabarti, 2014), specifically P53 deacetylase activity, leading to the accumulation of acetylated P53. Acetylated P53 causes downstream signaling impeding a cells ability to make energy in the mitochondria through oxidative phosphorylation (Imai & Guarente, 2014). This decrease in mitochondrial activity serves to maintain or even boost NAD^+/NADH levels by reducing the amount of damaging reactive oxygen species (ROS) produced by the mitochondria affecting DNA and consuming NAD^+ in the repair process. While initially protective, this downregulation of mitochondrial activity may leave older cells less able to deal with chronic stresses (Schutt, Aretz, Auffarth, & Kopitz, 2012). Decreased NAD^+/NADH and increased NAM have been theorized to be an early AMD initiators (Zhou, Luo, & Zhang, 2018). The RPE cell is responsible for maintaining the photoreceptors, clearing outer segments, and recycling retinoids which are energy intensive processes, this makes the RPE especially vulnerable to changes in metabolism and DNA repair over time. Low intracellular NAD^+/NADH and high NAM could lead to metabolic dysregulation over time, and potentially the onset of AMD.

NAD^+ Regulated Pathways and Biosynthesis

The sirtuin family of proteins are responsible for a host of behaviors related to metabolism (Gaur et al., 2017), and have been implicated in AMD (Zhou et al., 2018). One study showed that single nucleotide polymorphism in the Sirt1 gene, a member of sirtuin family, was associated with AMD progression in humans (Chen, Zhai, Zhang, Teng, & Yao, 2015). A steady NAD^+ supply allows Sirt1 to regulate metabolic processes

and the activity of critical pathways including DNA repair and oxidative stress response. However, NAM can also bind to and inhibit Sirt1 its function, making NAM clearance a cell priority (Avalos et al., 2005). NAD^+ can be produced from regular diet precursors, such as nicotinamide riboside (NR), tryptophan, and nicotinic acid (NA) (Figure 3). These precursors are processed into nicotinamide mononucleotide (NMN) and later metabolized into NAD^+ through the activity of nicotinamide nucleotide adenylyl transferases (NMNAT1-3)(Garten et al., 2015).

NMNAT1 mutations cause Leber congenital amaurosis 9 (LCA9), a form of photoreceptor degeneration resulting in congenital blindness, demonstrating the critical role of NAD^+ in the retina (Chiang et al., 2012). Interestingly, in mammals most of the NAD^+ supply comes from the salvage pathway (Fang et al., 2017). This pathway (Figure 3) converts NAM into NMN via the rate limiting enzyme nicotinamide phosphoribosyltransferase (NAMPT, Figure 3). Next, NMNAT1 used NMN as a substrate to generate NAD^+. NAMPT is the key regulating enzyme in the salvage pathway (Lin et al., 2016). Inhibiting NAMPT's ability to reduce NAM levels and generate new pools of NAD^+ could model an aging phenotype in cells. Other research demonstrates inhibition of NAMPT both *in vivo* and *in vitro* to be toxic, and therefore requires precautions to differentiate cell death from an aging or disease-relevant phenotype (Zabka et al., 2015).

Cellular Model of NAMPT Inhibition

FK866 is a commercially available NAMPT inhibitor used to study modulations of NAD^+/NADH levels affecting cellular functions like metabolism and Sirtuin activity. NAD^+/NADH depletion leads to defects in metabolism by removing important substrates

for the tricarboxylic acid cycle (TCA) and glycolysis (Du et al., 2016). Examining how NAMPT inhibition through FK866 affects a spontaneously immortalized human RPE cell line (ARPE-19) could prove useful modeling age-related changes seen in non-ocular tissues (Srivastava, 2016). ARPE-19 cells are commonly used in pre-clinical *in vitro* studies in the Ophthalmology field. However, teasing apart which pathway changes are due solely to the reduction of available NAD^+/NADH and which are due to the increase of intracellular NAM is difficult (Fouquerel et al., 2014; Massudi et al., 2012). Supplementation of NAD^+/NADH precursors, like NR or NMN, has shown to be protective in some aging models of disease (Gong et al., 2013; Hou et al., 2018). Supplementing cells with NAD^+/NADH precursors in combination with the NAMPT inhibitor FK866 should allow for the accumulation of NAM while maintaining a pool of usable NAD^+/NADH via biosynthetic pathways that do not engage NAMPT (Figure 3)

Research Aims and Hypothesis

NAD^+ decline and NAM accumulation are aging hallmarks associated with age-related disease (Johnson & Imai, 2018) and may be one of the earliest events in AMD combining with other risk factors—such as genetics, lifestyles, and the environment—can contribute to disease progression.

We hypothesize that the age-driven disruption of NAD^+ biosynthesis will lead to imbalance in the NAD^+/NAM ratio and result in downregulation of genes controlled by the Sirtuin family. Given that this family of proteins is a key regulator of mitochondrial activity and metabolism, the downregulation of these genes will result in a change in

functional metabolism readouts. Restoring the proportion of NAD^+ can recover those metabolic readouts.

We aim to find a dose of NAMPT inhibitor FK866 effectively inhibiting NAMPT without causing widespread cell death in an RPE cell line, ARPE-19. We will then characterize that dose of FK866 using molecular marker and functional readouts to build an understanding of how NAM accumulation dysregulates ARPE-19 cells. Subsequently, we will try to recover the baseline cell phenotype using doses of known precursors to NAD^+/NADH. While precursor supplementation addresses the decline of NAD^+/NADH from the inhibition of salvage pathway, NAM should steadily accumulate inside the ARPE-19 cells, further changing metabolic activity.

Chapter II.

Materials and Methods

Tissue Culture and Media Conditions

Human retinal pigment epithelium (ARPE-19, ATCC, catalogue CRL-2302) were cultured in T-150 flasks (Corning, 430825) until confluent in growth media consisting of Dulbecco's Modified Eagle Medium Nutrient Mixture F12 (DMEM/F12, Gibco, 11320033), 10% heat-inactivated fetal bovine serum, and 1% Penicillin-Streptomycin (ThermoFisher Scientific, 15140122). Cells were cultured in a humidified chamber with 5% CO_2 at 37°C and received fresh media changes once weekly. Cultures were maintained at confluence in for 1 week before expanding into subsequent assay plates. All experiments were performed using cells at passages 9-12. During passaging, cells were dissociated in 5mL of 0.05% Trypsin EDTA (Gibco, 25300054) for 10 minutes at 37°C. 5mL of fresh media was then added to the cells, and cell counts were determined using a Vi-Cell XR (Beckman Coulter, Brea, CA). Cells were seeded at 30,000 cells per cm^2 in DMEM/F12 for all plates, and no greater than a 1:3 ratio was used for the maintenance of cells in T-150 flasks. 6- and 12-well plates were used for protein isolation and RNA experiments. Black, clear-bottom 96- and 384-well plates were used for the imaging studies. White, opaque 96- and 384-well plates were used for the luminescence assays. SeaHorse 96-well plates were used for all metabolism studies. Cells were cultured for two weeks after seeding before switching to experiment media.

Different cell culture media can have drastic effects on cellular metabolism and gene expression (Cantor et al., 2017), so we chose to compare two types of media for all our assays. The first media is the recommended growth media by ATCC for ARPE-19 cells: Dulbecco's Modified Eagle Medium Nutrient Mixture F12 (DMEM/F12, Gibco, 11320033), 10% fetal bovine serum, and 1% Penicillin-Streptomycin (ThermoFisher Scientific, 15140122). The second media is our low-glucose media, referred to as "Phys", comprised of Dulbecco's Modified Eagle Medium (DMEM, Gibco, A14430-01), 1mM L-Glutamine (Sigma, G3126-100G), 6mM D-Glucose (Gibco, 15023021), 2mM L-Lactate (Alfa Aesar, L14500), 100μM Sodium Pyruvate (Gibco, 11360070), 1% Penicillin-Streptomycin (ThermoFisher Scientific, 15140122), and 10% fetal bovine serum. A full list of the differences between the media can be found in Table 1. To ensure adequate nutrient supply, media was replaced every two days. Media exchange frequency was kept consistent for the DMEM/F12 controls. ARPE-19 cells were maintained in Phys media for 5 days before the beginning of each experiment. Media comparisons occurred on the same assay plate to minimize variability unless otherwise noted.

FK866 and Precursor Treatments

The NAMPT inhibitor FK866 hydrochloride hydrate was supplied from Millipore Sigma (F8557-25MG) and dissolved in dimethyl sulfoxide (DMSO, ThermoFisher Scientific, D12345). Nicotinamide Riboside (Cayman Chemicals, 1341-23-7), Nicotinamide (Sigma, 72340), and Nicotinamide Mononucleotide (Sigma, N3501) were dissolved in ddH_2O and stored at -20℃.

Fresh aliquots of FK866 were used to create a compound plate of 6X concentration to add to ARPE-19 cells. FK866-titrated curves were prepared in a

compound master plate at 6X final concentration. This master plate was used for compound addition to all 96- and 384-well assays with final assay concentrations of FK866 ranging from 10μM to 0.001μM. The dose response of the precursors NR, NAM, and NMN ranged from 1mM to 1μM. The treatment duration ranged to 1, 3 or 5 days. After the completion of the dosing, plates were prepared for subsequent assays.

Cell Viability Assays

Previous experiments in our group have shown that using different cell viability measurements with different modalities can help confirm the toxicity—or lack thereof—in compounds. Our studies used luminescence-based and imaging-based assays to determine the efficacy of the tested compounds. The first cell viability assays were performed in 384-well format in plates optimized for luminescence. The CellTiterGlo kit (Promega, G7572) was used to measure cell viability via the presence or absence of intracellular adenosine triphosphate. After treatment, cells were washed once with phosphate buffered saline (PBS, Gibco, 14190-136), incubated with the CellTiterGlo detection reagent for 10 minutes, and then scanned for luminescence on the Envision 2105 (PerkinElmer, Waltham MA).

The second cell viability assays were performed using black-wall, clear-bottom optical 384-well plates. After treatment, cells were incubated with a staining solution consisting of 2μM Ethidium Homodimer-1 (ThermoFisher Scientific, E1169), Calcein AM (ThermoFisher Scientific, C3100MP), 1% Bovine Serum Albumin (BSA, VWR, VWRV0332-500G), and 1:5,000 Hoechst (Sigma 94403). Cell death was induced in positive control wells with 0.25% Digitonin (ThermoFisher Scientific, BN2006) for 10

minutes prior to staining. Cells were incubated with viability stain for 45 minutes then imaged at 20X on the InCell 2200 high content imager (General Electric Healthcare Life Sciences, Marlborough, MA). Images were analyzed using Cell Profiler (Broad Institutes, Cambridge, MA).

A custom cell profiler pipeline was used to identify Ethidium Homodimer-1 stained nuclei, Hoechst positive nuclei, and the area covered by the calcein AM staining. Only the percentage of dead cells per well was reported. Both ethidium homodimer-1 and Hoechst label DNA and can lead to overlapping signals. A merged image was used to quantity the total number of cells (live or dead) in an image, and the total number of ethidium homodimer-1 positive cells was used to calculate the percentage of dead cells per well. An overview of this process can be seen in Figure 4.

Reverse Transcription and Quantitative Polymerase Chain Reaction

Plates for RNA isolation were washed 1X with RNAase free water to remove any excess FBS that may affect downstream processing. RNA was isolated from ARPE-19 cells using the AllPrep DNA/RNA/Protein Mini Kit (Qiagen, 80004). RNA concentration was determined by NanoDrop 2000 (ThermoFisher Scietific), and samples were normalized before cDNA preparation. CDNA was prepared using the High-Capacity cDNA reverse transcriptase transcription kit (ThermoFisher Scientific, 4368814). qPCR assays were performed in 384-well PCR plates (Applied Biosystems, 4343814) using the primers listed in Table 2. TaqMan qPCR was run on the Applied Biosystems ViiA 7 using the ViiA 7 software. mRNA expression of target genes was normalized to the endogenous control *RPLP1*. Fold change of gene expression was calculated using the $2^{-\Delta\Delta CT}$ method.

Protein Isolation and Western Blotting

Protein was isolated from ARPE-19 cells first by washing cells with phosphate buffered saline (PBS) and then lysed with 300uL for 6-well plates or 150uL for 12-well plates of RIPA cell lysis buffer (Cell Signaling Technology, 9806) with protease (Roche, 04693159001) and phosphatase inhibitors (Southern Biotech, 0201-01) as well as PMSF (Sigma, P7626). Cells were scraped and further disrupted using the Qiagen Tissue Lyser for 20 minutes at 30rps. Total protein of lysates was quantified by Bradford assay using Coomassie Protein reagent (Pierce, 23200). Protein was normalized, and samples were run via SDS-PAGE on 17- or 10-well gels (ThermoFisher Scientific, NP0321BOX), transferred to standard polyvinylidene fluoride (PVDF) membranes, and blocked for 1 hour using 3% bovine serum albumin (BSA) TBST. Primary antibodies were diluted 1:1,000 and incubated overnight at 4℃. The following day, membranes were washed 5X with Tris-Buffered Saline Tween-20 (TBST) and incubated with secondary HRP antibodies 1:5,000 for 120 minutes. Membranes were washed again 5X with TBST and then exposed to Supersignal West Femto ECL Kit (ThermoFisher Scientific, 34095). Membranes were imaged using the FluorChem E (Bio-techne, Minneapolis, MN) and analyzed using NIH ImageJ software. A full list of antibodies, dilutions, and catalogue numbers can be found in Table 3.

Total NAD^+/NADH Measurement

A NAD^+/NADH Glo kit (Promega, G9072) was used to quantify total NAD^+/NADH following the provider's instructions. A 1-second integration time was used for each well.

SeaHorse ATP Production Rate Assay

A buffered Krebs-Ringer Phosphate Solution (KRPS) with a known buffering capacity was used per vendor instructions to determine the ATP production rate using the Agilent extracellular flux analyzer (Guntur et al., 2018; Mookerjee, Gerencser, Nicholls, & Brand, 2018). Following treatment with FK866 or precursors, media was switched to compounds free DMEM/F12 of Phys for 30 minutes before 2X washes in KRPS. Cells were kept in buffered KRPS with 10mM Lactate and 0.5mM L-Carnitine for 30 minutes before the assay. The KRPS used was buffered to a pH of 7.4 and used to create all inhibitor/substrate solutions. The assay plate sat overnight at 37°C in XF Calibrant (Agilent, 100840-000) before the day of the assay. Once the assay plate was calibrated in the XF96 machine, the basal Oxygen Consumption Rate (OCR) and Extracellular Acidification Rate (ECAR) were measured. These rates are used in the further calculations for the basal ATP production. After 3 measurement cycles, 5.5mM of glucose was added to the cells. The addition of glucose and the subsequent changes in OCR and ECAR allowed us to calculate the induced ATP production rate of our cells following treatment. Next, cells were treated with 2µM Oligomycin (Sigma, #75351-5mg) to inhibit the production of ATP through ATP synthase, leading to an increase in lactate and ECAR. Then 2µM Antimycin-A (Sigma, A8674-25mg) and 2µM Rotenone (Sigma, R8875-1g) were added to completely inhibit OXPHOS by uncoupling the electron transport chain. Lastly, the cells were labeled with 5µM Hoechst to normalize our SeaHorse data with total cell numbers per well.

The ATP Rate assay protocol can be found in Table 4. After the completion of the assay, total nuclei were counted via the Cytation5 plate reader. Total cell number was

used to normalize the SeaHorse data. The ATP rate assay report generator was used to generate the mitochondrial and glycolysis ATP production fractions, which were graphed in GraphPad Prism.

Statistical Analysis

All graphs were made in GraphPad Prism 7 software. Results are mean ± standard error of mean unless otherwise stated. Statistical analysis was performed in GraphPad with significance defined as $p < 0.05$ using either two- or three-way analyses of variation, or multiple t-tests. Metabolism studies utilized a three-way analysis of variation with a Bonferroni's multiple comparisons post-test, to test if there was an interaction effect between the three variables we were testing.

Chapter III.

Results

Metabolic Effects of NAMPT Inhibition on ARPE-19

NAMPT Inhibition Decreases Intracellular NAD/NADH and ATP but Does Not Cause Cell Death

Our first objective was to identify an FK866 dose that significantly reduced NAMPT activity without effecting cell viability. Because glucose can change cellular metabolism, we used media with either standard (DMEM/F12, glucose 25 mM, Table 1) or physiological (Phys media, 6 mM glucose, Table 1) glucose concentrations. We used high-content imaging to quantify ARPE-19 viability after 1, 3 or 5 days of NAMPT inhibition. Fresh FK866 (up to 10 μM) and media were added every other day. Cytotoxic digitonin was used as a positive control to induce cell death at the end of the challenge. Viable cells were detected with calcein AM and dead cells with ethidium homodimer (EthD). Studies were imaged at a 20X magnification and analyzed with a Cell Profiler pipeline (Figure 4).

Cell death was not detected with any of the FK866 doses tested (Figure 5) at 1, 3 or 5 days. The digitonin positive control group showed over 60% EthD positive cells, as expected. In contrast, all FK866 doses tested were positive for calcein AM. Our results confirmed other published reports (Jadeja et al., 2018) that have also reported minimal cell death at the FK866 concentrations tested.

NAMPT Inhibition Decreases Intracellular NAD^+/NADH in ARPE-19 Cells Treated with FK866 for 3 or 5 Days

We used a commercially available NAD^+/NADH measurement kit to determine the efficacy of FK866-mediated NAMPT inhibition. Compared to naive ARPE19, significantly diminished NAD^+/NADH (Figure 6) was detected starting at 0.01953 μM FK866 in DMEM/F12 ($p=0.033$) and 0.0098 μM in phys media ($p=0.018$).

NAMPT Inhibition Decreases Intracellular ATP in ARPE-19 Cells Treated with FK866 for 3 or 5 Days

Next, we asked how low NAD^+/NADH affected cellular metabolism by measuring ATP production. Dose-response time course studies in both media for 1, 3 or 5 days using a commercially available kit that uses a luciferase-based detection agent to measure ATP (CellTiterGlo, Promega). Decreased ATP was not observed in cells treated with FK866 or DMSO for 1 or 3 days relative to naïve ARPE-19 (N=2 studies). On day 5, significantly lower ATP levels were detected with doses as low as 0.0781 μM (Figure 7, 68% decrease in DMEM/F12 and 62% in phys media, $p=0.0009$ and 0.0032, respectively). Higher doses further decreased ATP. Cells challenged with DMSO (the compound solvent) had little-to-no effect on ARPE-19 intracellular ATP.

The studies described in this section show that FK866 efficiently blocks NAMPT activity resulting in lower NAD^+/NADH and metabolic stress (low ATP) without inducing ARPE-19 death. We selected a 1μM FK866 dose for subsequent studies. Because the presence of glucose did not affect the cellular response, we decided to perform gene expression studies in phys media unless otherwise indicated.

Metabolic and Gene Expression Consequences of NAMPT Inhibition by FK866

NAD^+/NADH Depleted Cells Have Inhibited Metabolism

ATP depletion associated with NAMPT inhibition suggests that ARPE-19 treated with FK866 are in a state of metabolic crisis. Oxidative phosphorylation (OXPHOS) and glycolysis, the major ATP synthesis pathways use NAD^+/NADH as coenzymes. Glycolysis requires NAD^+/NADH for the conversion of glyceraldehyde-3-phosphate to 1,3-*bis*phosphoglycerate via glyceraldehyde 3-phosphate dehydrogenase (GAPDH, Figure 8A). OXPHOS uses NAD^+/NADH in the citric acid cycle, reductive carboxylation, and pyruvate dehydrogenase steps to generate ATP by transferring electrons from either NADH or $FADH_2$ to O_2 (figure 8B). We used the SeaHorse ATP rate assay to investigate the effect of NAMPT inhibition on OXPHOS and glycolysis.

First, we assessed baseline metabolism for ARPE-19 cultured in either DMEM/F12 or Phys media conditions. Cells cultured in media with higher concentrations of glucose are more likely to use glycolysis, as glucose is readily available. However, the RPE cell must undergo glycolysis sparingly, to maintain a steady supply of glucose to the outer segments. To represent this function in culture, we need to force our ARPE-19 cells to use OXPHOS for their ATP generation, by reducing the amount of glucose in the culture media. Because the difference in glucose content between these media would modify the readouts, we also tested Phys media with the same glucose concentration as DMEM/F12 (17 mM). Our results show that when cultured in DMEM/F12, ARPE-19 prefer to engage glycolysis (Figure 9) as glucose is abundant. In contrast, ARPE-19 cells in Phys media with a physiologically relevant glucose concentration (6 mM) use their mitochondria for the majority of ATP generation,

but retain their ability to use glycolysis in acute high glucose environments (Figure 9B). Mitochondrial and glycolysis ATP production in Phys media with 17mM glucose is indistinguishable from DMEM/F12 media (Figure 9B, p=0.8144, and 0.0933 respectively), suggesting that the main driver towards preferential OXPHOS seen in Phys is low glucose.

ARPE-19 cells treated with 1μM FK866 in DMEM/F12 had a modest reduction in ATP generation basally that did not recover in the presence of glucose (Figure 10A). These cells also had a preference for OXPHOS as a pathway for ATP generation over glycolysis, even in the high glucose environment. This observation suggests that when faced with a NAD^+ crisis, OXPHOS is the most efficient pathway to generate ATP, even in conditions that would typically favor glycolysis.

The effects observed were larger on ARPE-19 cells treated with FK866 in Phys media. Unable to generate ATP through glycolysis and having the smallest fraction of ATP generation through their mitochondria, these cells were able to boost their glycolysis in the presence of excess glucose but were not able to reach control levels (Figure 10B, $p < 0.0001$). The induced ATP production rate measures the amount of ATP cells can generate after the reintroduction of glucose, essentially measuring whether or not the cellular machinery required for ATP production can still function. The lack of available NAD^+/NADH for glycolysis explains why the induced ATP production rate in both media conditions never reach the same levels as the naive controls. Cells have the ability to change their metabolism when conditions in the environment change, like decreasing Sirtuin activity when stressed. Internal mechanisms may regulate cellular metabolic activity as a means of damage control (Schutt et al., 2012).

Loss of Mitochondrial Genes Observed in NAMPT Inhibited ARPE-19 Cells

We analyzed mitochondrial marker expression (*COX4I1* and *TOMM20*) to support the SeaHorse-detected metabolic changes (Figure 11). The expression of both genes decreased after a 5-day challenge with 1μM FK866. This observation supports decreased ATP generation via OXPHOS, and suggests that NAMPT inhibition may affect mitochondrial biogenesis. Alternatively, decreased mitochondrial gene expression may be an attempt to preserve NAD^+/NADH or regulate metabolic activity to reduce cellular damage (Schutt et al., 2012).

NAMPT Inhibited ARPE-19 Cells Decrease Expression of Creatine Kinase Pathway Genes

We next asked how ARPE-19 produce sufficient ATP to maintain cellular functions. ATP synthesis via the creatine kinase pathway relies on intracellular phosphocreatine concentrations and may not be affected by NAMPT inhibition. TaqMan measurement of two genes on this pathway (*CKB* and *CKMT2*) demonstrated minimal changes (Figure 12). A slight decrease in *CKB* expression was observed in the DMEM/F12 group treated with FK866 for 5 days ($p=0.0286$), and an increase in *CKB* expression was observed in the Phys group treated with FK866 for 5 days ($p=0.0036$). The increase seen in the Phys media suggests that the cells are trying to generate more ATP through the creatine kinase pathway. Additional experiments are needed to confirm this observation.

NAMPT Inhibition Alters ARPE-19 Gene Expression

AMD progression has been associated with mitochondrial dysfunction and an energetic crisis that can result in loss of RPE identity (Feher et al., 2006). TaqMan quantitative PCR was used to analyze the expression of genes critical for RPE identity (*Otx2* and *Mitf*, figure 13A-B) and function (visual cycle and photoreceptor outer segment phagocytosis: *Rlbp1, Lrat* and *Mertk*, figure 13C-E). Our results demonstrate with 1μM FK866, expression of these genes decreased as early as three days, continuing to decrease at day five, suggesting decreased NAD^+/NADH leads to loss of RPE identity and function (Figure 13, A-E). Remarkably, these changes preceded significant decreases in NAD^+/NADH levels.

In vivo work suggests that murine RPE de-differentiation associates with decreased *Lrat* and *Rlbp1* expression and increased *Mitf* (Zhao et al., 2011). Our results that ARPE19 de-differentiation may not engage the same pathway as murine cells.

Senescence is a cellular process associated with energetic crisis such as an ATP decrease (Jadeja et al., 2018). TaqMan analysis of the classical senescence markers *Ctgf*, *Cdkn2a,* and *Cdkn1a* did not detect an increase of the first two genes (Figure 14 A-B). Interestingly, NAMPT inhibition did not affect *Cdkn1a* expression at any time point (Figure 14C). NAD-dependent sirtuins regulate P53, which is necessary to activate P21 the *Cdkn1a* protein product. The constant expression of both *CDKN1A* and *CDKN2A* suggests that low NAD^+ does not affect p53 activity in ARPE-19.

Low NAD^+/NADH Does Not Change Total SIRT1 or Acetyl-P53 Protein

Because the previous results suggest that NAMPT inhibition is not sufficient to decrease sirtuin activity, we decided to analyze active p53 (acetylated P53, Ac-p53) and

sirtuin-1. Western blot analysis of ARPE-19 cells treated with FK866 for 3 or 5 days showed no decrease in SIRT1 protein when compared to Alpha-tubulin (data not shown). Ac-p53 blots showed no significant changes in protein level.

NAD^+ Precursor Supplementation

Dosing Precursors Alone Does Not Affect Cell Viability

Cells can generate their own pools of NAD^+/NADH by internalizing precursors like Nicotinamide (NAM), Nicotinamide Mononucleotide (NMN), and Nicotinamide Riboside (NR)(Fang et al., 2017; Imai & Guarente, 2014). NMN and NR feed into the NAD^+ biosynthesis pathway after NAMPT (Figure 3), NAM does not. Extracellular NAM can be converted into NMN or NR via CD73 before it can be internalized, or directly internalized through an unknown receptor (Fang et al., 2017). Separating out the effects of internalized extracellular NAM versus converted NAM will be difficult. Adding these compounds to NAMPT inhibited cells may help tease apart the differences between high intracellular NAM, and low NAD^+/NADH, by allowing cells to generate useable NAD^+ while preventing them from recycling NAM.

Staining with ethidium homodimer showed that dosing with NAM, NMN or NR did not induce cell death at any concentration tested (1 mM to 1 μM Figure 15).

NAD^+ Precursor supplementation in combination with FK866

ATP Depletion Can Be Recovered with Precursor Supplementation

Next, we explored whether NAD^+/NADH precursors are able to prevent the metabolic crisis and RPE-specific marker loss observed in NAMPT-inhibited ARPE19. Precursor addition to ARPE19 treated with FK866 (1μM) re-established ATP to naive levels at the highest concentrations of NAM, NMN, or NR tested (Figure 16) and did not induce cell death in either media conditions (Figure 17).

NAM was able to rescue ARPE-19 cells at the higher concentrations even though NAMPT is inhibited, suggesting that either NAMPT inhibition is not total, or extracellular NAM is metabolized into a different precursor that can then be utilized downstream of NAMPT. A greater than 50% recovery was observed in the 250 μM NAM treated cells in both media ($p=0.0039$, and 0.0002 compared to Naive levels). NMN had the best recovery profiles in each experiment with complete or partial recovery seen in some of the lower concentrations. A dose of 31.25μM NMN was able to rescue more than 50% of ATP signal in both media ($p=0.0382$, and 0.0901 when compared to Naive levels). NR did not recover ATP in the lower concentrations. Going forward we decided to focus solely on NMN supplementation for cell rescue because it exhibited the best profiles in the cell death modalities.

ARPE19 express transporters for NMN but not for NR

In support of the viability findings, TaqMan data confirmed that *SLC18A*, a proposed NMN transporter, is expressed by RPE and its expression is not affected by FK866-mediated NAMPT inhibition (Figure 18). This corroborates our previous findings that NMN was much better at recovery in the FK866 treated cells than NR. In contrast, *NT5E,* a gene associated with NR transport, is downregulated by NAMPT inhibition.

Media conditions had an effect on the stratification of the precursors with NMN having the greatest effect in the Phys media compared to NAM and NR in the same media. Both NT5E and SLC12A8 are purported to be the receptors that internalize extracellular NAM or NR (Grozio et al., 2019), and they decrease their expression in response to NAD^+/NADH depletion. This suggests the presence of a mechanism that modulates the internalization of NAD^+ precursors in the presence of excess NAM.

Gene Expression and Protein Levels Return to Baseline with NMN Supplementation in NAMPT Inhibited Cells

Taqman gene expression analysis of ARPE-19 cells treated with both 1μM FK866 and 20 μM of NMN had recovery of their RPE markers (Figure 19). The NMN supplementation reversed the decline in gene expression seen in NAMPT inhibition, which may mean that the loss of RPE identity in our cells was mainly due to the loss of available NAD^+/NADH. However, limited sample size precluded meaningful statistical analysis. Repeating this study with larger samples sizes can help separate the effects of low NAD^+/NADH and high intracellular NAM

ATP Production Rates Can Be Recovered with NMN Supplementation

The extracellular flux assay showed no changes in the metabolic profile of ARPE-19 cells treated solely with NMN for 5 days in either media condition (Figure 20). FK866 was able to significantly reduce the basal mitochondrial ATP production rate in the Phys media ($p<0.0001$), but not in the DMEM/F12 ($p>0.9999$). This effect is driven by the glucose conditions in the media. Basal glycolysis ATP production rate was significantly

reduced in the DMEM/F12 group treated FK866 when compared to untreated controls ($p<0.0001$). Combination treatment of FK866 and NMN was able to recover the basal glycolysis ATP production rate in DMEM/F12 ($p=0.0116$).

FK866 significantly reduced induced glycolysis in both media conditions ($p<0.0001$ for both conditions). Combination treatments recovered the glycolysis ATP production in both media conditions, but was still significantly reduced in compared to untreated controls ($p=0.0081$, and $p=0.0004$ for DMEM/F12 and Phys respectively). Even though the treated cells cannot recycle NAM into NMN to make NAD^+, they still perform their metabolic functions normally.

NAD^+/NADH Levels Can Be Recovered with NMN Supplementation

Treating ARPE-19 cells alone with 20μM NMN did not significantly boost the intracellular concentration of NAD^+/NADH in either media condition (Figure 21). However, in combination with 1μM FK866, NAD^+/NADH concentrations recovered to almost ~50% their normal levels at 5 days. Recovery in DMEM/F12 was higher (64%, $p<0.0001$), than in Phys media (42%, $p<0.0001$). These cells should have enough NAD^+/NADH to undergo glycolysis and OXPHOS, unlike the FK866 only treated cells. CTG data run in the same conditions also shows an increase in intracellular ATP which should correlate with increased metabolism (Figure 22).

Chapter IV.

Discussion

Significance of Results

Our results show that intracellular levels of NAD^+/NADH are crucial to maintaining a healthy ARPE-19 cell. Decreasing the amount of available NAD^+/NADH rapidly downregulates the expression of genes associated with RPE identity and activity in the visual cycle (Figure 13), potentially leaving them to de-differentiate if given enough time. These de-differentiating RPE cells will no longer perform RPE-specific duties, like making melanin to absorb light, Declining NAD^+/NADH levels have been witnessed in a variety of human tissues, including the brain (Zhu, Lu, Lee, Ugurbil, & Chen, 2015) and liver (Fang et al., 2017; Okabe, Yaku, Tobe, & Nakagawa, 2019). Although no studies have shown decreased NAD^+/NADH levels in the human eye, given how crucial maintaining those levels are (Zabka et al., 2015; Zhu et al., 2015), it is a reasonable assumption that there is a age-related decline in the retina and/or RPE layer.

Depletion of NAD^+/NADH was also seen to down regulate TOMM20, (Figure 11) a marker for mitochondria, and in human RPE cells there is a reduction in the number and volume of mitochondria (Feher et al., 2006). A chronic depletion of NAD^+/NADH over time may lead to the decline in mitochondria and total mitochondrial function in AMD patients. It may be necessary for RPE cells to maintain mitochondrial function and biogenesis by maintaining a supply of NAD^+/NADH. Feher et al observed a decline in RPE mitochondria volume and number as age increases with the loss accelerated in patients with AMD. Suggesting that there is something wrong with AMD patient's RPE cells manifesting earlier than their age-matched counterparts. Having a reduced number

of mitochondria in an aged RPE cell would severely compromise its ability to perform any of the tasks relating to supporting photoreceptors let alone mediating the damage from internalizing outer segments and processing toxic lipids. These conditions could lead to loss of function, with the RPE cells making less ATP from their own mitochondria and relying heavily on glycolysis.

One mechanism that could compensate for the loss of ATP would be upregulating the creatine kinase genes. Creatine kinases use a reversible enzymatic reaction to generate phosphocreatine and adenosine diphosphate (ADP) or creatine and ATP. Since cells treated with FK866 cannot generate ATP through glycolysis or oxidative phosphorylation they could switch to consuming phosphocreatine to generate ATP. However, our gene expression assays showed no significant increases in creatine kinase expression in our ARPE-19 cells treated with FK866 (Figure 12). Pools of available phosphocreatine may have already been consumed earlier our assays, so no changes in gene expression were required. Further investigation into how ARPE-19 cells survive low ATP environments in necessary.

In naïve conditions, ARPE-19 cells that are in DMEM/F12 source the majority of their ATP from glycolysis in spite of the similar expression of TOMM20 in RPE in Phys media. This suggests cells in DMEM/F12 have mitochondria available to use but do not need to be as efficient with their glucose. The differences seen in their metabolic profile are dependent on distinct media conditions (Figure 9).

Supplementing our NAMPT inhibited ARPE-19 cells with NMN showed signs of reversing the phenotype in both our SeaHorse assays and our qPCR data. NAMPT inhibition pushed the ARPE-19 cells into a metabolic crisis, completely shutting down

glycolysis as a metabolic pathway even in the high-glucose environment of the DMEM/F12 media. What little glycolysis the ARPE-19 cells performed in the Phys media was even further reduced by NAMPT inhibition. In both conditions, the ARPE-19 cells dramatically adjust their ATP production rate, which can also be seen by CellTiter-Glo (CTG). NMN supplementation rescued these changes. We bypassed the inhibited NAMPT enzyme and supplemented our cells with precursors for NAD^+/NADH, which the ARPE-19 cells subsequently used for glycolysis and OXPHOS. With the cells free to use either pathway, they recovered their ATP production and level, and a normal metabolic phenotype.

We also saw that supplementation has the ability to rescue baseline expression of RPE-specific genes. Looking at the RPE cell marker genes, *OTX2*, *MITF*, and *LRAT*, we saw recovery to an RPE like state with the supplementation of NMN (figure 20). *SLC18A1*, a proposed transporter for NMN also recovers to normal expression level with the supplementation of NMN. The gene expression data in combination with the SeaHorse data show that the decreases in metabolic function and the stress associated with low NAD^+/NADH can be reversed at 5 days. Demonstrating that the functional changes are not permanent and that an ARPE-19 cells fate can be changed back to baseline is interesting in understanding how potentially low NAD^+/NADH in the eye can be changed *in vivo*.

Although we were able to reverse the phenotype induced by NAMPT-inhibition, we were not able to observe any distinct change that we could attribute solely to NAM accumulation inside the ARPE-19 cell. NAM has been shown to inhibit sirtuins which should have created a feedback effect on metabolism, which we did not observe. ARPE-

19 cells treated with FK866 and precursors were still able to perform both glycolysis, and more critically oxidative phosphorylation. Though the FK866 and precursor treated cells never reached their naïve controls the differences in both the basal and induced rates were not as large as the NAMPT inhibited cells. Confoundingly, we did observe decreases in metabolism in ARPE-19 cells treated solely with NAM (figure 23), showing the limitation of our model.

Research Limitations

ARPE-19 are a cell line that has been used in AMD research for many years. Despite their advantages (easy to culture, readily accessible, expression of RPE markers, and able to phagocytize outer segments), there are considerable limitations to this system. Inherent genome instability in the cell line has led to some studies abandoning their use for *in vitro* research (Fasler-Kan et al., 2018). ARPE-19 cells also lack important RPE specific genes, like RPE65, which make them a less-than-ideal choice. Combined with batch-to-batch variation, ARPE-19 cells may not be the best choice for retinal research. Utilizing induced-pluripotent stem cells (iPSCs) are a better option for more fully recreating RPE cells in culture but also comes with donor-to-donor variation. Gene expression in iPSC-RPE cells is more in line with what is seen in humans and also have the ability to polarize and become pigmented over time. These differences make them a far better candidate for modeling the complex nature of the RPE cell in humans. Other researchers have also tried to create models of AMD in iPSC-RPE cells driven by dysregulated Sirt1 (Golestaneh et al., 2016). Although they are more difficult to maintain, expand, and utilize in wide-scale experimentation they are the most accurate cell lines, in

terms of gene expression and function, we have available and could be used to confirm findings before testing *in vivo*.

Another important difference in our studies is that the RPE cell does not exist in a vacuum inside the eye: it is part of a complex network of interconnected cells performing a variety of functions. Growing ARPE-19 cells in a plate inherently misses choroidal circulation, and the interaction with photoreceptors. Recreating this network is the main obstacle to *in vitro* research in ophthalmology and, specifically, AMD. In addition, oxygen concentrations also differ widely on each side of the RPE cell, with the photoreceptor side being relatively hypoxic and the choroid side being oxygen rich. Polarizing, feeding outer segments, and growing ARPE-19 cells in trans-wells can overcome some of these problems but at a cost of reproducibility. Translating our data from cells to animals may be difficult, but a majority of the enzymes associated with NAD^+ are conserved among different species (Gaur et al., 2017). NAMPT inhibition in rats has led to retinal degeneration within one week (Zabka et al., 2015), and this effect is seen in homozygous NAMPT knockout mice (Lin et al., 2016), showing that using our model of low NAD^+/NADH *in vivo* may be unattainable and strongly suggesting that NAMPT function is critical for photoreceptor and RPE survival *in vivo*.

Our low NAD^+/NADH and increased intracellular NAM hypothesis would be better served if we had a way to measure intracellular NAM. Liquid chromatography-mass spectrometry (LC/MS) is the gold standard for measuring small metabolites but is technically challenging. Because LC/MS was not easily accessible, we chose to use p53 acetylation as a readout for sirtuin activity in the presence of excess NAM. Although modulation of sirtuins regulation of the acetylation of p53 is well documented (Gaur et

al., 2017), we were unable to corroborate this finding with western blots. This is most likely due to the limitations of the utilized detection system. Utilizing better detection methods, and a more thorough validation of the antibodies could have yielded results more in line with the current literature. With these limitations in mind, we believe there is merit to further examining the effects of low NAD^+/NADH and/or increased NAM *in vitro* and *in vivo*.

Further Study

Our results show that low NAD^+/NADH *in vitro* decreases metabolic function and disruption of RPE identity and mitochondrial markers and can be recovered with NMN supplementation. Testing other pathways or functions *in vitro* would be enlightening. A remaining question raised by our work is if cells with lower NAD^+/NADH have lower trans-epithelial resistance due to lower expression of RPE specific markers (Figure 13). The RPE cell is a tight monolayer of cells preventing the free flow of nutrients and molecular signals from the choroidal circulation to the photoreceptors. Compromised barrier function in RPE cells *in vivo* leads to angiogenesis, as seen in the latest stages of AMD. We know that NAMPT-inhibited cells have little spare ATP which could inhibit their ability to phagocytize outer segments. Failure to properly process photoreceptor outer segments could lead to lipid build up like drusen. Adding fatty acid oxidant inhibitor etomoxir, allow us to see if ATP generated from fatty acid catabolism supports survival of ARPE cells challenged with NAMPT inhibition.

We know that dosing with a NAMPT inhibitor *in vivo* is toxic given enough time (Zabka et al., 2015); knockout of NAMPT is embryonically lethal (Lin et al., 2016); and partial knockdown of NAMPT is able to disrupt retinal structure. Together these suggest

an important role for NAMPT in life and in the eye. Seeing if partial NAMPT inhibition leads to similar changes in gene expression and molecular markers *in vivo* and if these changes can be altered with NMN or other precursor supplementation may make for an interesting case to further study low NAD^+/NADH in humans. Lin et. al. generated a Cre recombinase NAMPT knock down in rods and cones of mice and saw a profound drop in their function when NAMPT was completely removed. Performing a similar study in with RPE cells may provide useful information on how the RPE specifically handles a low NAD^+/NADH environment. We know that the retina is incredibly sensitive to NAMPT inhibition, and it may try to maintain levels of NAD^+/NADH better than RPE cells.

Study of donor human eyes is challenging as NAD^+/NADH are unstable, breaking down quickly, making measurements non-representative of the living tissues due to post mortem time frame from death to eye harvest. Linking these changes in metabolites to ocular tissues will therefore be challenging. Currently, human donor eyes can be obtained 6 or more hours after death. A newly-developed MRI technique that allows NAD^+/NADH level measurement in human brains was recently documented in the literature (Zhu et al., 2015), and could be a novel tool in discovering NAD^+/NADH's role in degenerative diseases. Applying this technique to human eyes would be no small feat but could help determine if retinal NAD^+/NADH declines with age, and if there are differences between AMD and non-AMD patients. Since this technique is non-invasive it could be used to track changes in NAD^+/NADH over time in healthy patients, and how patients with AMD respond to different treatments.

Conclusions

NAD^+/NADH biosynthesis and its role in regulating downstream gene expression associated with metabolism, cell fate, and function make it an interesting area of research. Our work shows that *in vitro* a decline in bioavailable NAD^+/NADH can modulate metabolic function in ARPE-19 cells, and these losses can be partially reversed by replenishing those pools of NAD^+/NADH by precursors supplementation. Although we tried to recapitulate findings seen in human disease our model system needs more work to bridge the changes seen in AMD and the accumulation of NAM. Further characterizing low NAD^+/NADH in the human retina may yield interesting pathways and potential therapies for AMD.

Appendix 1.

Tables

Table 1. List of media components.

Component	DMEM/F12 (mM)	DMEM "Phys" (mM)
Amino Acids		
Glycine	0.25	0.4
L-Alanine	0.0499997	0
L-Arginine hydrochloride	0.69905216	0.39810428
L-Asparagine-H2O	0.05	0
L-Aspartic acid	0.05	0
L-Cysteine hydrochloride-H2O	0.09977272	0
L-Cystine 2HCl	0.09996805	0.20127796
L-Glutamic Acid	0.05	0
L-Glutamine	2.5	1
L-Histidine hydrochloride-H2O	0.14990476	0.2
L-Isoleucine	0.41580153	0.8015267
L-Leucine	0.45076334	0.8015267
L-Lysine Hydrochloride	0.4986339	0.7978142
L-Methionine	0.11570469	0.20134228
L-Phenylalanine	0.2150303	0.4
L-Proline	0.15	0
L-Serine	0.25	0.4
L-Threonine	0.44915968	0.79831934
L-Tryptophan	0.04421569	0.07843138
L-Tyrosine disodium salt dihydrate	0.21375479	0.39846742
L-Valine	0.4517094	0.8034188
Vitamins		
Biotin	1.4344263E-5	0
Choline chloride	0.06414285	0.02857143
D-Calcium pantothenate	0.0046960167	0.00838574
Folic Acid	0.0060090707	0.0090703
Niacinamide	0.016557377	0.03278688
Pyridoxine hydrochloride	0.009771844	0.01960784
Riboflavin	5.0184503E-4	0.00106383
Thiamine hydrochloride	0.0064391694	0.01186944

Vitamin B12	5.0184503E-4	0
i-Inositol	0.07	0.04
Inorganic Salts		
Calcium Chloride (CaCl2) (anhyd.)	1.05045	1.8018018
Cupric sulfate (CuSO4-5H2O)	5.20E-06	0
Ferric Nitrate (Fe(NO3)3"9H2O)	1.24E-04	2.48E-04
Ferric sulfate (FeSO4-7H2O)	0.0015	0
Magnesium Chloride (anhydrous)	0.301474	0
Magnesium Sulfate (MgSO4) (anhyd.)	0.407	0.8139166
Potassium Chloride (KCl)	4.157333	5.3333335
Sodium Bicarbonate (NaHCO3)	29.02381	44.04762
Sodium Chloride (NaCl)	120.6121	110.344826
Sodium Phosphate dibasic (Na2HPO4) anhydrous	0.500141	0
Sodium Phosphate monobasic (NaH2PO4-H2O)	0.452899	0.9057971
Zinc sulfate (ZnSO4-7H2O)	0.0015	0
Other Components		
D-Glucose (Dextrose)	17.50556	6
Hypoxanthine Na	0.015031	0
L-Lactate	0	2
Linoleic Acid	1.50E-04	0
Lipoic Acid	5.10E-04	0
Phenol Red	0.02152	0
Putrescine 2HCl	5.03E-04	0
Sodium Pyruvate	0.5	0.1
Thymidine	0.001508	0

List of all the components in the media used in our studies.

Table 2. List of Primers

Gene	Assay Id
Dedifferentiation	
ACTA2	Hs00426835_g1
CDKN1A	Hs00355782_m1
CDKN2A	Hs00923894_m1
CKB	Hs00176484_m1
CKMT2	Hs00176502_m1
COX4I1	Hs00971639_m1
CTGF	Hs00170014_m1
LRAT	Hs00428109_m1
MERTK	Hs01031979_m1
MITF	Hs01117294_m1
MTOR	Hs00234508_m1
NNMT	Hs00196287_m1
NT5E	Hs00159686_m1
OTX2	Hs00222238_m1
RLBP1	Hs00165632_m1
RPLP1	Hs01653088_g1
SLC12A8	Hs00226405_m1
TOMM20	Hs00740685_sH
VMAC	Hs00418522_m1

List of all the primers used for quantitative PCR used in our studies.

Table 3. List of Antibodies

Protein	Catalog Number	Dilution
Primary Antibodies		
SIRT1	Cell Signaling Technologies #8469	1:1,000
Acetylated P53	Cell Signaling Technologies #2525S	1:1,000
Secondary Antibodies		
Anti-Mouse HRP	Cell Signaling Technologies #7076	1:1,000
Anti-Rabbit HRP	Cell Signaling Technologies #7074	1:1,000

List of all the antibodies for western blots used in our studies.

Table 4. ATP Rate Assay Protocol

Step	Number of Cycles	Mix (min)	Wait (min)	Measure (min)
Baseline	3	1:00	1:00	3:00
Glucose	2	1:00	0:00	2:00
Oligomycin	2	1:00	0:00	2:00
Rotenone/Antimycin-A	2	1:00	0:00	2:00
Hoechst	1	1:00	0:00	0:00

Description of the ATP rate assay performed in our lab.

Appendix 2.

Figures

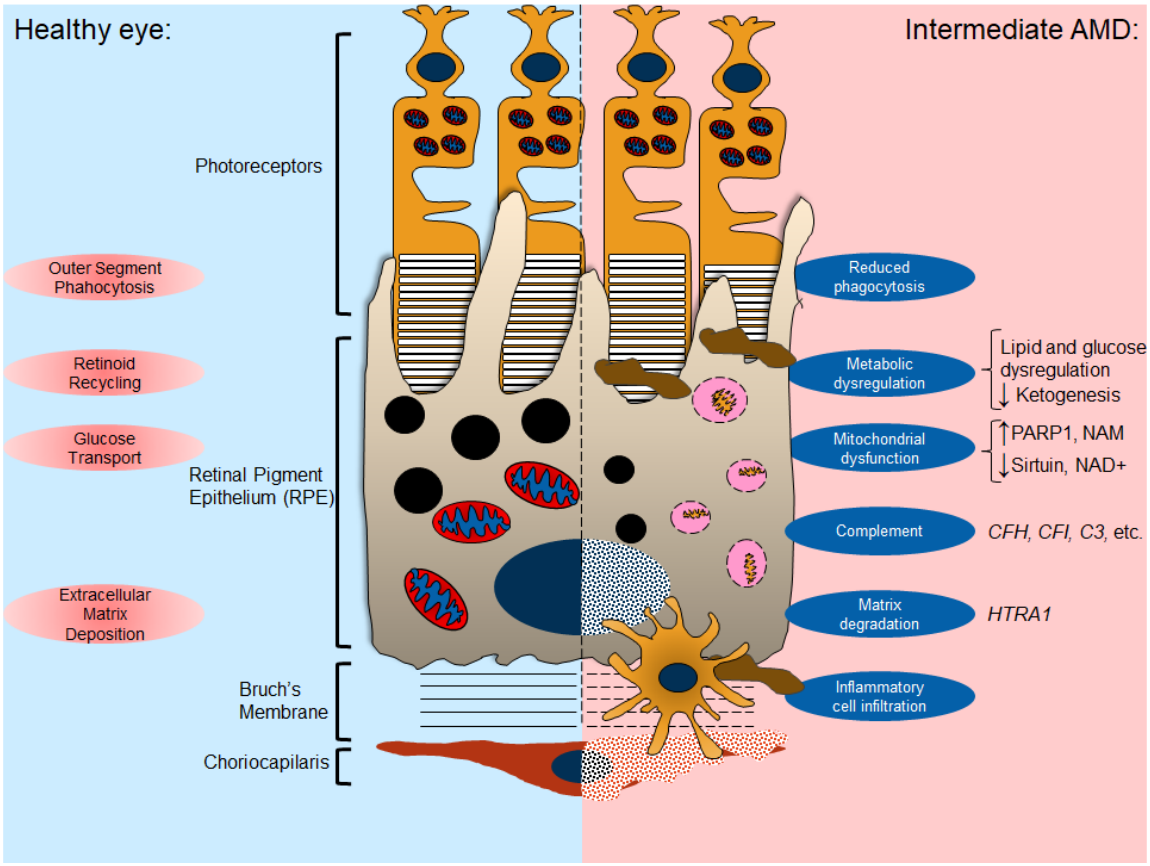

Figure 1. The RPE and Photoreceptor Interface.

Pictured are some of the interactions of the Retinal Pigment Epithelium and the photoreceptor outer segments (Toops, Tan, & Lakkaraju, 2014). In the healthy eye (left) the RPE is responsible for a variety of homeostatic processes. However, in intermediate AMD (right) the RPE cannot maintain those functions, leading to lipid build up in the form of drusen on either side of the RPE cell, smaller less efficient mitochondria, differences in melanin pigmentation, infiltration of macrophages to the subretinal space, a porous Bruch's membrane, and choriocapillaris dropout. Left unchecked these changes can lead to neovascular AMD and/or geographic atrophy.

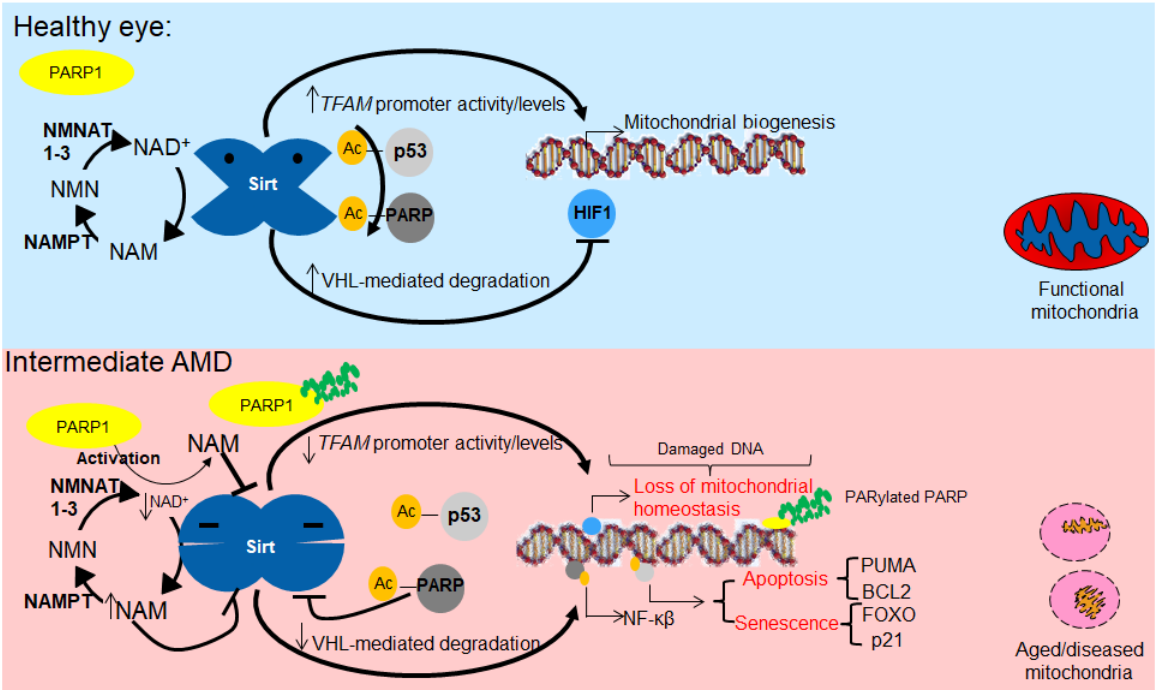

Figure 2. Hypothesis for Aging Decreasing Mitochondrial Function

Hypothesis of how the imbalance of NAD/NADH to NAM in intermediate AMD changes mitochondrial activity. In a healthy eye (top), a balance of NAD^+/NADH and NAM is maintained allowing for proper Sirt activity. Sirt deacetylases P53, and PARP, and promotes mitochondrial biogenesis through TFAM (Transcription Factor A, mitochondria). PARP1 is responsible for repairing DNA damage, and required NAD^+ to function. VHL (Von-Hippel Lindau) is responsible for the degradation of Hif1 (Hypoxia inducible factor), and, in a healthy eye, genes under Hif1's control are kept regulated by VHL. As we age DNA damage increase, bioavailable NAD^+/NADH decreases and NAM begins to accumulate. Accumulated NAM inhibits Sirt activity, which in turn decreases mitochondrial biogenesis. VHL degradation of Hif1 decreases, and genes associated with apoptosis and senescence begin to be expressed. This runaway loss of function decreases an RPE cells ability to maintain its homeostatic processes and the whole retina begins to degenerate.

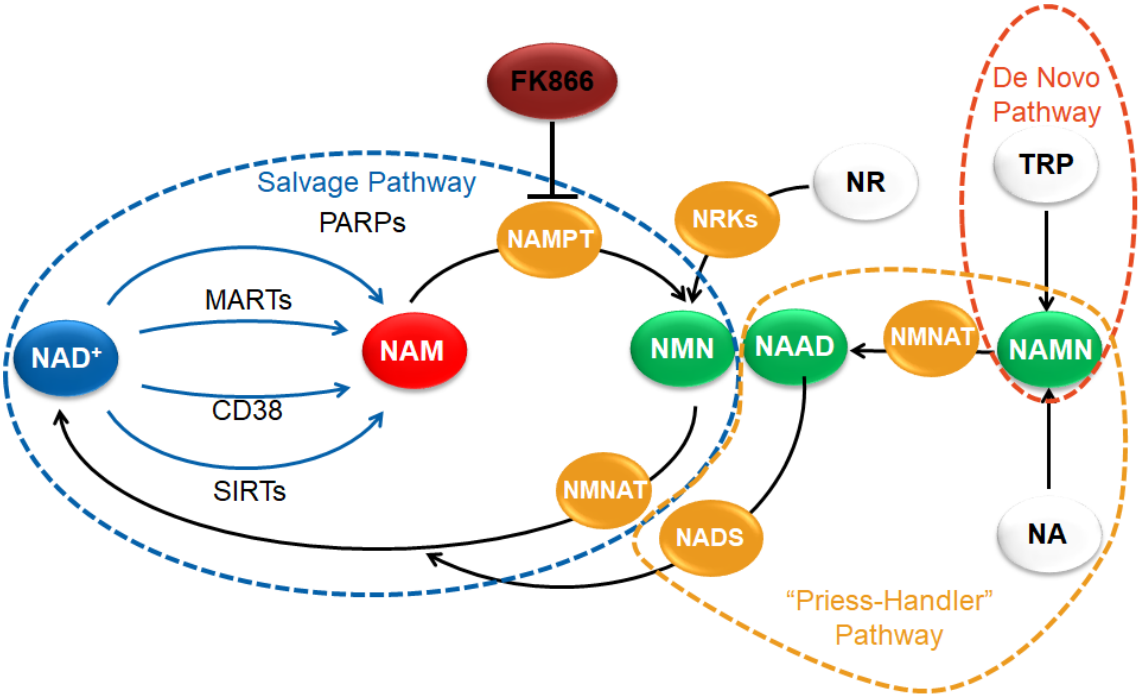

Figure 3. NAD^+ Biosynthesis Pathways Diagramed

NAMPT inhibition would reduce the amount of NMN that could be turned into NAD^+ by NMNAT1-3. This reduces the amount of NAD^+ available for NAD consuming reactions and redox reactions. Legend: CD38: Cyclic ADP-ribose hydrolase, MARTS: Mono ADP-ribose Polymerases, NA: Nicotinic Acid, NAAD: Nicotinic Acid Adenine Dinucleotide, NAD^+: Nicotinamide Adenine Dinucleotide, NADS: Nicotinamide Adenine Dinucleotide Synthetase, NAM: Nicotinamide, NAMN: Nicotinic Acid Mononucleotide, NAMPT: Nicotinamide Phosphoribosyltransferase, NMN: Nicotinamide Mononucleotide, NMNAT: Nicotinamide Mononucleotide Adenylyltransferase , NR: Nicotinamide Riboside, NRKs: Nicotinamide Riboside Kinases, PARPs: Poly (ADP-ribose) Polymerases, SIRTs: Sirtuins, and TRP: Tryptophan (Fang et al., 2017).

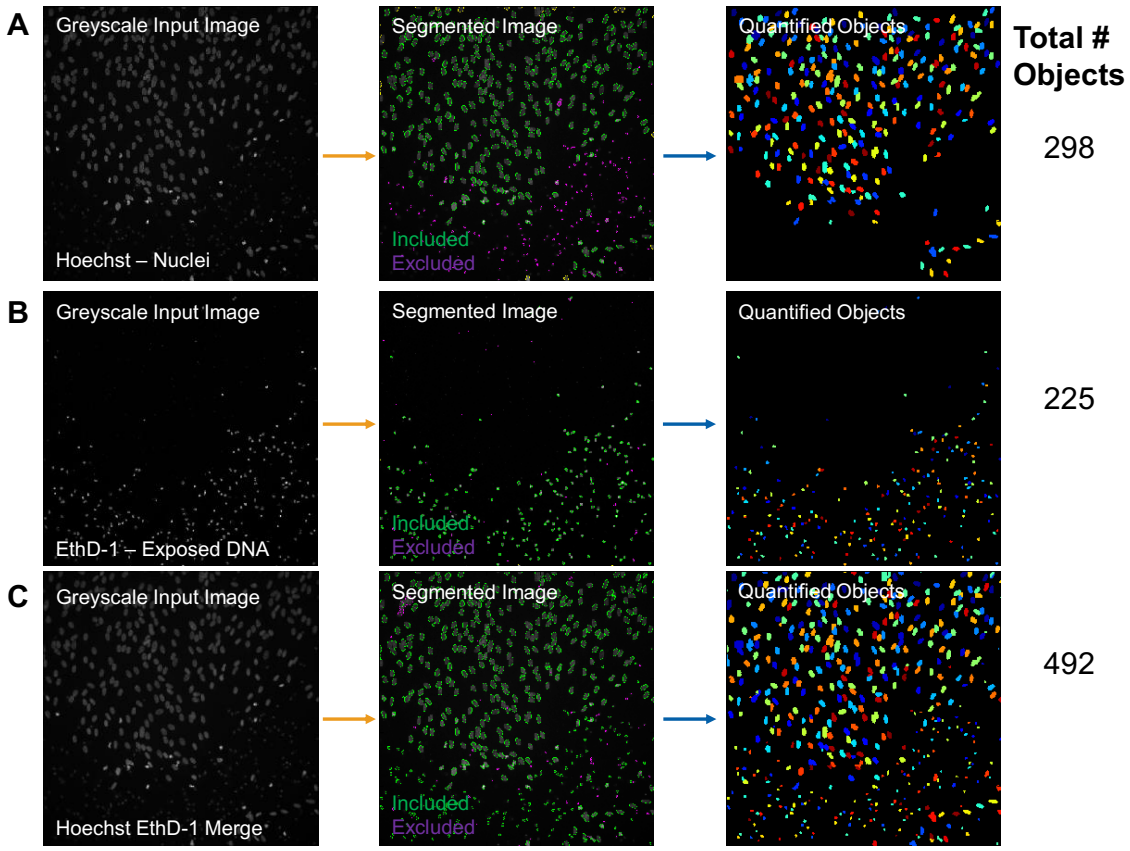

Figure 4. Cell Profiler Pipeline Overview

Cell profiler is used to capture the number of Hoechst (A) and Ethidium Homodimer-1 (B) positive nuclei images separately because both signals overlap, a combined object (C) total is used to determine the percentage of dead cell in a field. The inclusion/exclusion criteria were determined in previous studies, gating the objects on their size/area and their brightness. Automating the quantification process allows analysis of a typical study with a 1,000+ images in about ten minutes.

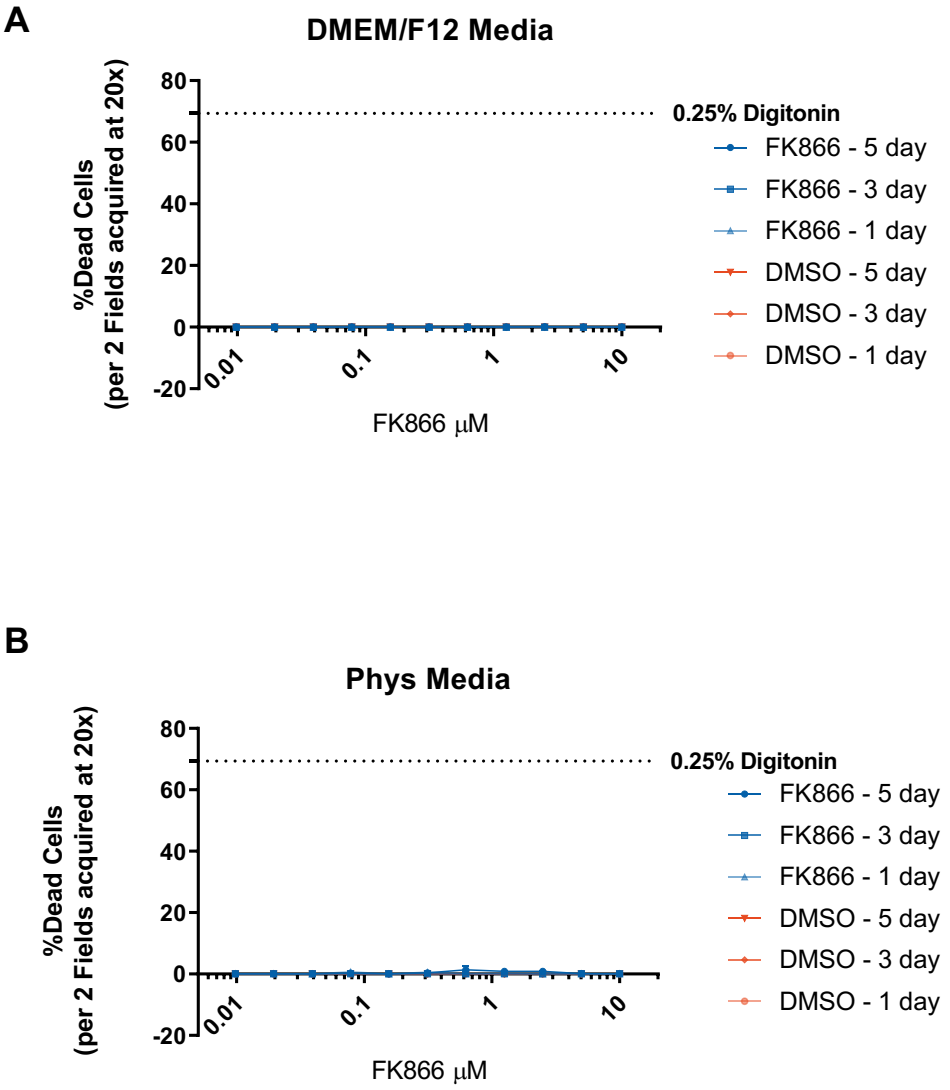

Figure 5. FK866-mediated NAMPT Inhibition is not Associated with ARPE-19 Death

Representative graphs of the average percentage of Ethidium Homodimer-1 positive cells per total cells per well cultured in DMEM/F12 (A) or Phys media (B). Treatment with positive control digitonin induced significant cell death (labeled line), in contrast, treatment with FK866 did not (n=2).

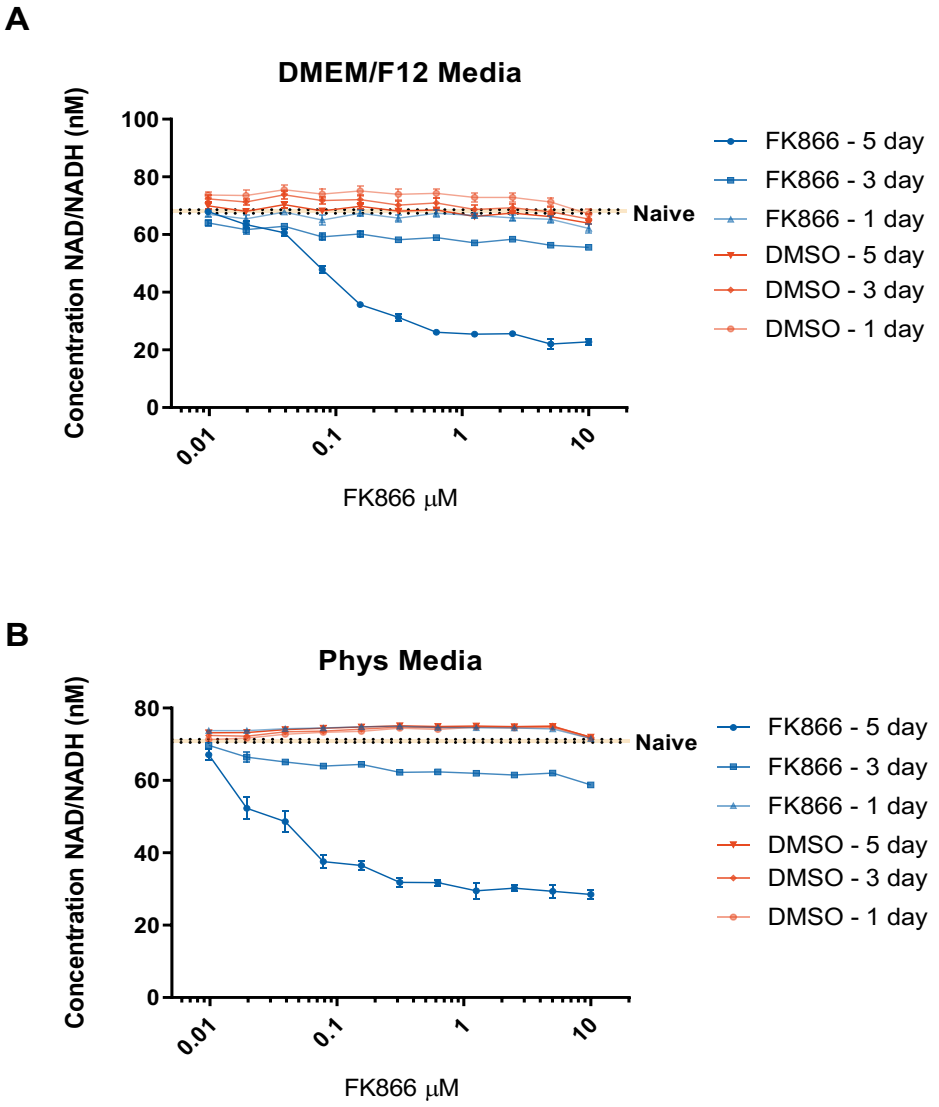

Figure 6. FK866 Treatment Diminishes Total NAD^+/NADH After 5 Days of NAMPT Inhibition

Five-day treatment with FK866 significantly reduces NAD^+/NADH concentration in ARPE-19 cell starting at ~0.019μM for DMEM/F12 (A, p=0.032776), and ~0.0097μM for Phys (B, p=0.018196). A ~60% reduction was observed at 1.25μM in both media (p=0.000003, and 0.000043 respectively). ARPE-19 cells were treated with a range of doses (0.01-10μM) for 1, 3, or 5 days in either DMEM/F12 or Phys. DMSO had no effect on total NAD^+/NADH in either media condition. Levels of total NAD^+/NADH were not different in naive cells in either media condition (n=2).

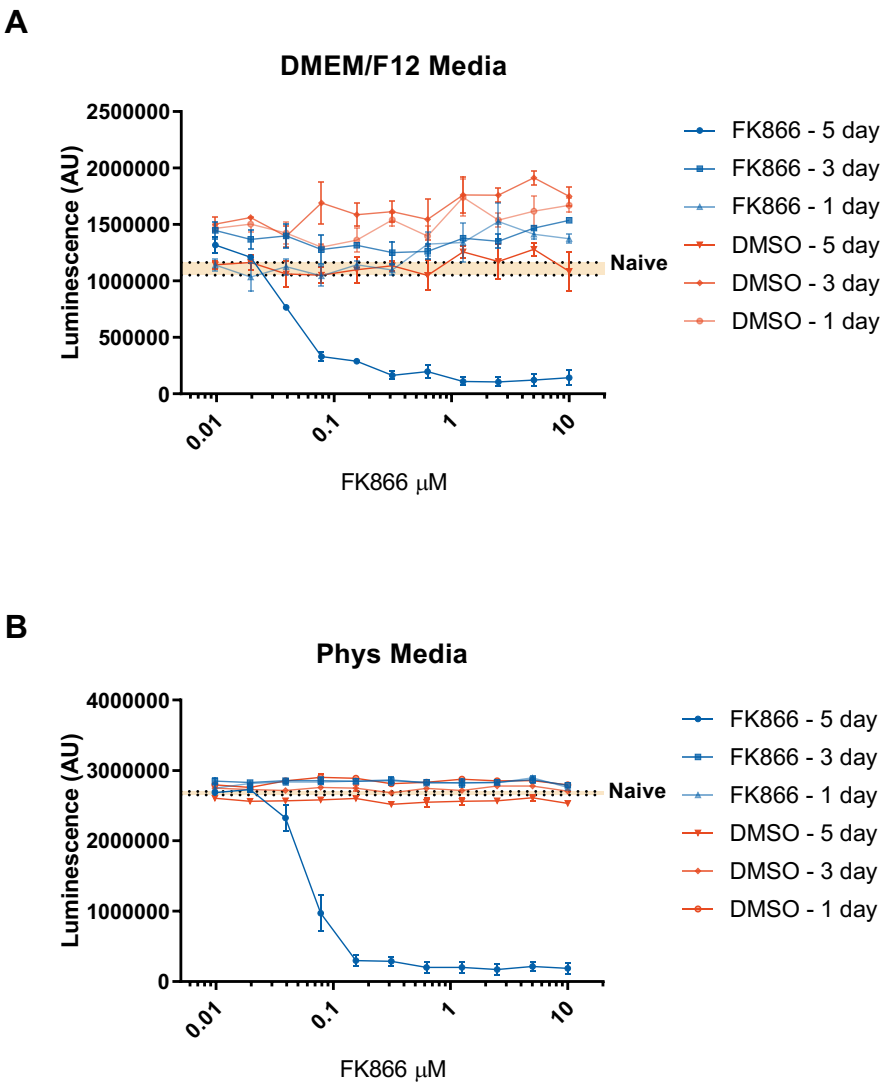

Figure 7. The NAMPT Inhibitor FK866 Deplete ATP in ARPE-19 After 5-Day Treatment

Representative CTG graphs of the presence of ATP levels after dosing with FK866 or equivalent volume of DMSO for the indicated times. Naive levels are represented by the yellow bounding box. ATP in ARPE-19 cells challenged with FK866 started to decrease after five days of treatment, in either DMEM/F12 (A) or phys media (B) but not the earlier time points. Both media had a 90% reduction in signal at 1.25μM FK866 (p=0.000063, and 0.000016). DMSO had little to no effect on ATP (n=2, t-tests used for significance).

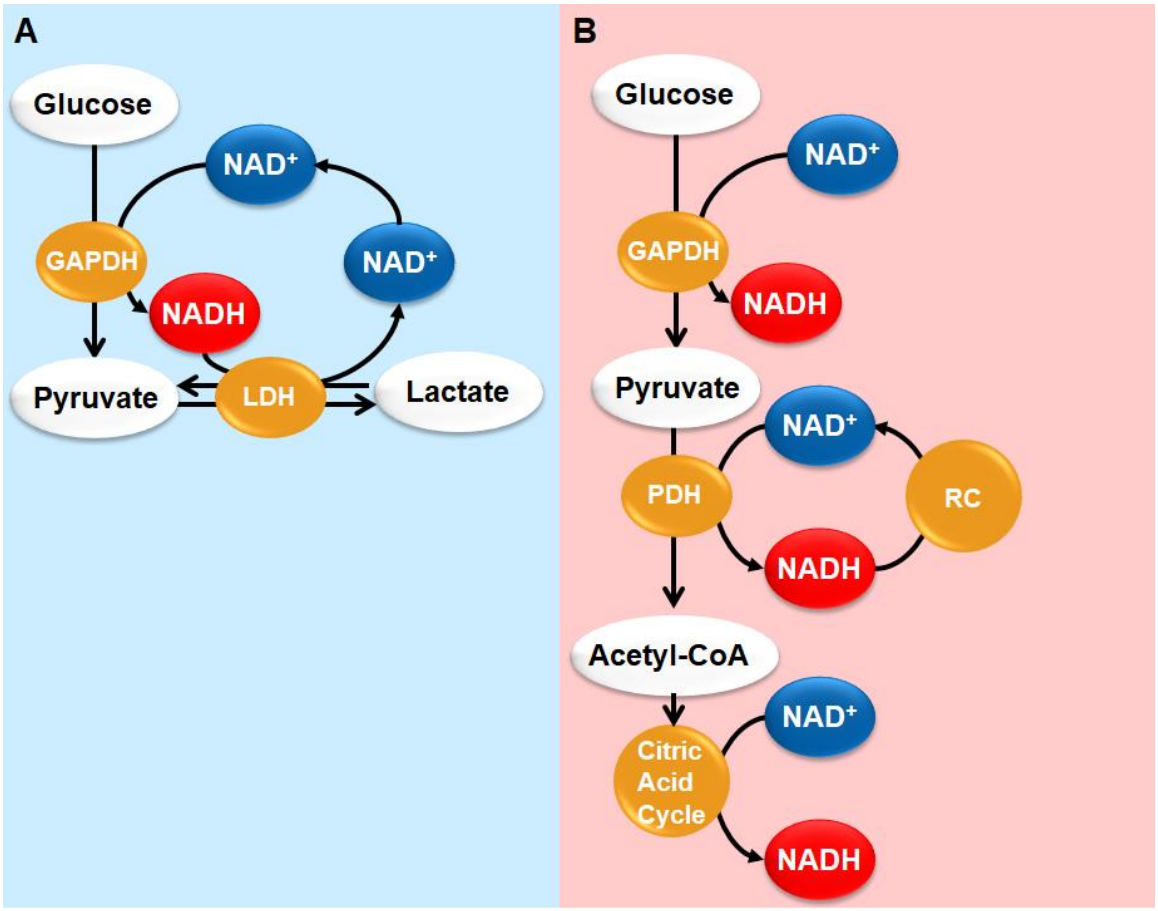

Figure 8. NAD^+/NADH Metabolic Redox Reactions

The enzymes that involve either NAD^+ or NADH in either glycolysis (A), or aerobic respiration (B). These enzymes do not consume NAD^+ or NADH, but recycle them into different redox states for use in other parts of the process (Houtkooper, Canto, Wanders, & Auwerx, 2010).

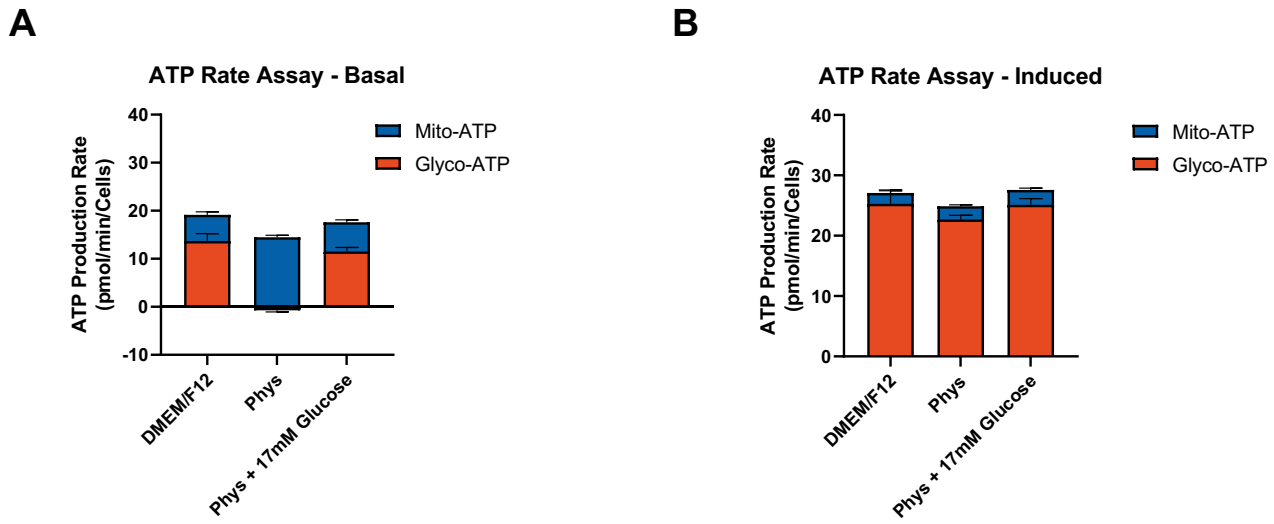

Figure 9. Lower Glucose Media Drives Mitochondrial ATP Production

(A) Basal ATP production was compared for DMEM/F12 (which contains 17 mM glucose, table 1); Phys (6 mM glucose, table 1) and Phys media supplemented with 17 mM glucose. Cells cultured in DMEM/F12 produce most of their ATP via glycolysis as glucose is abundant (first column). In contrast, ARPE-19 cultured in phys (low glucose) prefer to engage mitochondria (center column). Despite their preference for mitochondrial production, ARPE-19 in Phys media retain the ability to engage glycolysis in a high glucose environment (third column). (B) When ATP production is induced using 5.5mM glucose ARPE-19 engage glycolysis regardless of culture conditions. DMEM/F12 and Phys + 17mM Glucose are not significantly different from one another, in either glycolysis or mitochondrial ATP production rate (p=0.0933, and 0.8144 respectively). Significance determined by a two-way ANOVA with a Tukey's multiple comparisons test.

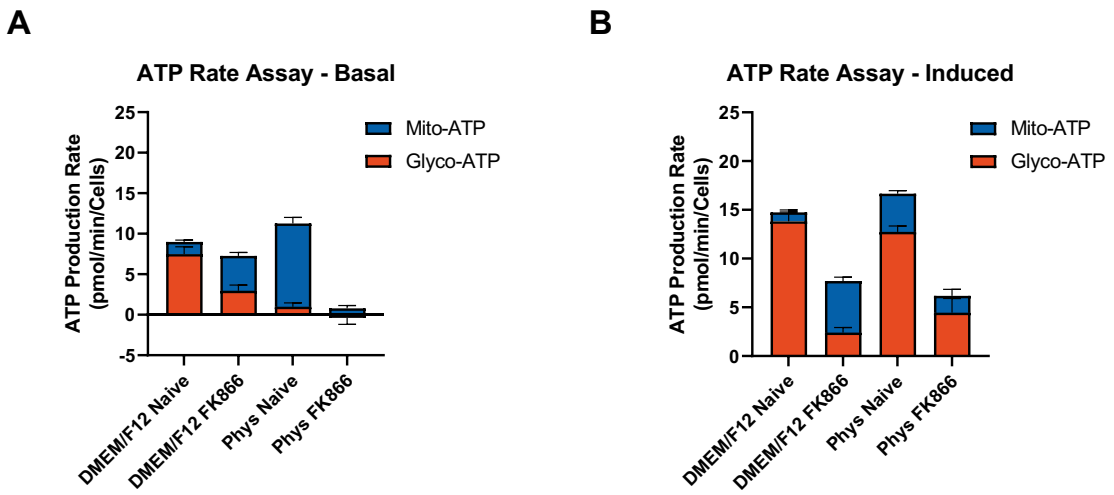

Figure 10. SeaHorse ATP Rate Assay Following FK866 Treatment

Representative extracellular flux studies show a shift in the ability of ARPE-19 cells to undergo both OXPHOS and glycolysis following NAD^+/NADH depletion in both basal and induced conditions. Significant reductions in metabolism were observed between treatment groups and their controls, using a three-way anova with a Bonferroni's multiple comparisons test (n=3). The three-way anova was used to determine the interaction effected between the multiple variables tested. Glycolysis ATP production was significantly reduced in response to FK866 treatment in both DMEM/F12 and Phys ($p<0.0001$ for both).

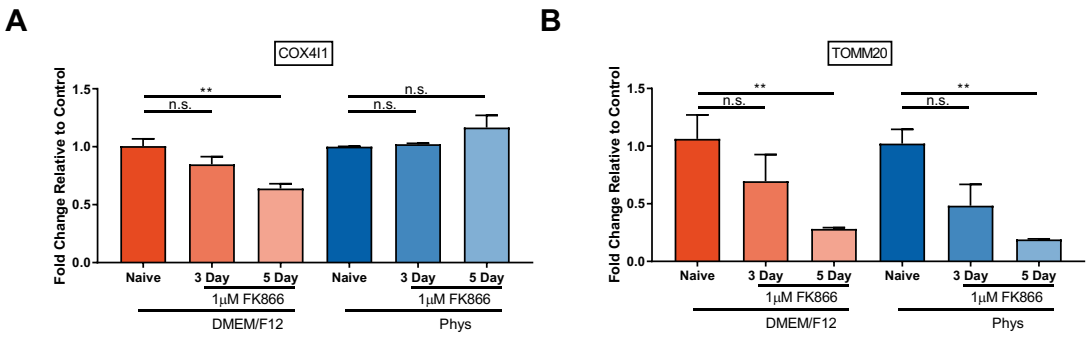

Figure 11. Mitochondria Related Gene Expression is Changed in NAD Depleted ARPE-19 Cells

COX4I1 (A) showed a decrease in expression in the DMEM/F12 group treated with FK866 for 5 days (p=0.0015). TOMM20 (B) also had a significant decrease in expression at 5 days (p=0.0094, and 0.0052 respectively). Significance was determined by a one-way ordinary ANOVA multiple comparisons test with findings reported as follows; p <0.05 (*), p <0.01 (**), p <0.005 (***), p <0.0001 (****).

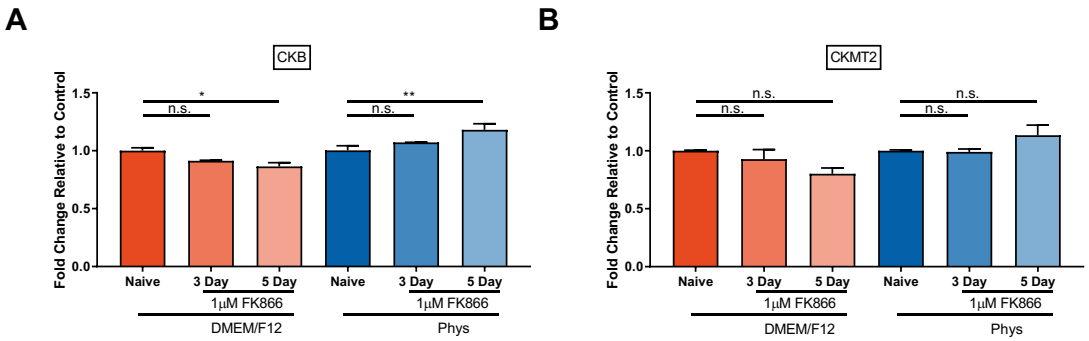

Figure 12. Metabolic Pathways are Slightly Modulated in NAD Depleted ARPE-19 Cells

(A) CKB was the only creatine kinase we examined that showed slight differences in gene expression after being dosed with FK866 for 5 days in both media conditions (p=0.0286, and 0.0036 respectively). CKMT2 (B) showed no differences. Significance was determined by a one-way ordinary ANOVA multiple comparisons test with findings reported as follows; p <0.05 (*), p <0.01 (**), p <0.005 (***), p <0.0001 (****).

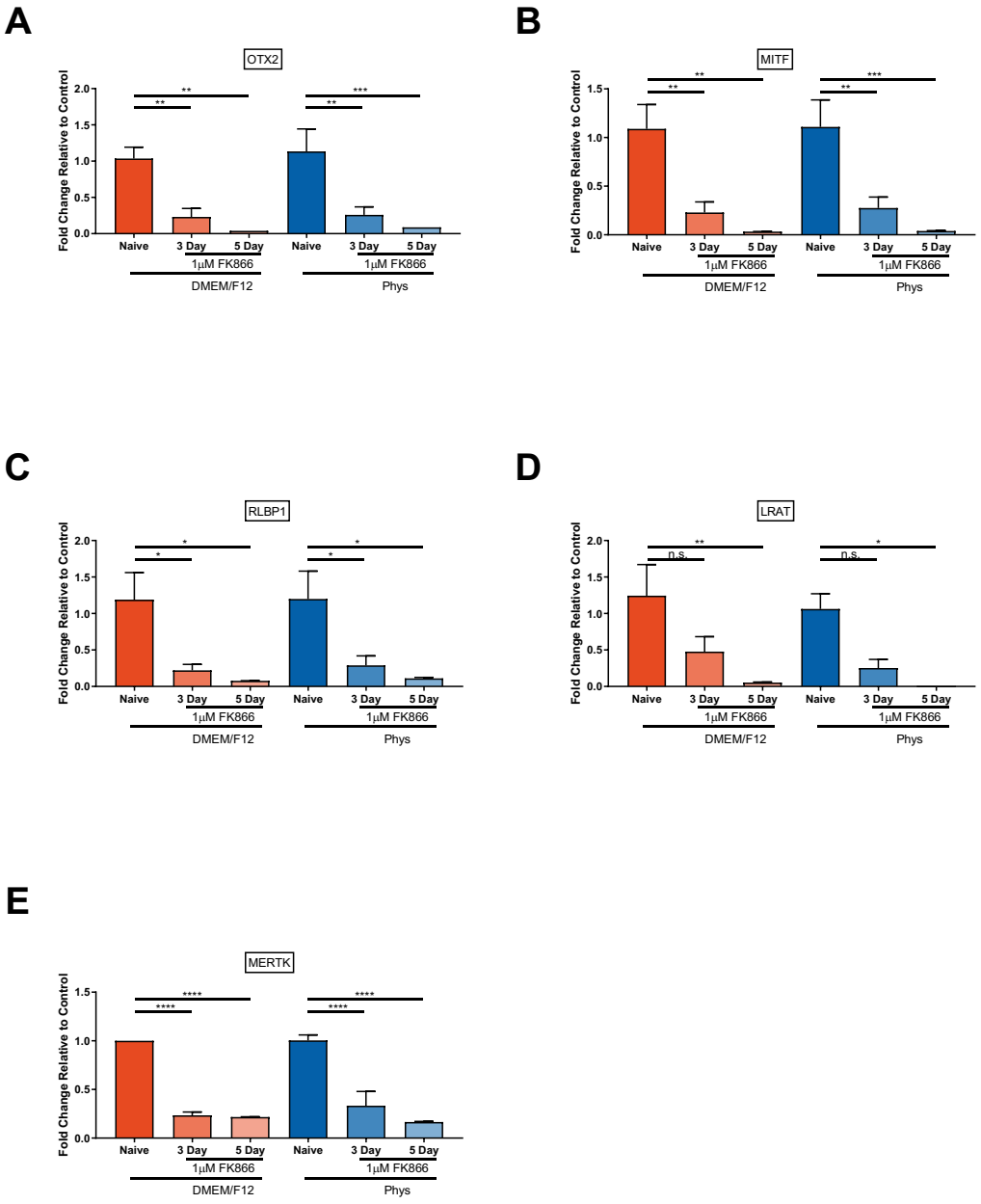

Figure 13. NAMPT Inhibition Reduces RPE-specific Gene Expression

FK866-mediated NAMPT inhibition reduces the expression of genes associated with RPE differentiation (OTX2 and MITF, top row), visual cycle (RLBP1 and LRAT, middle row) and outer segment phagocytosis (MERTK, bottom row). Media conditions did not affect the described result. Significance was determined by a one-way ordinary ANOVA multiple comparisons test with findings reported as follows; p <0.05 (*), p <0.01 (**), p <0.005 (***), p <0.0001 (****).

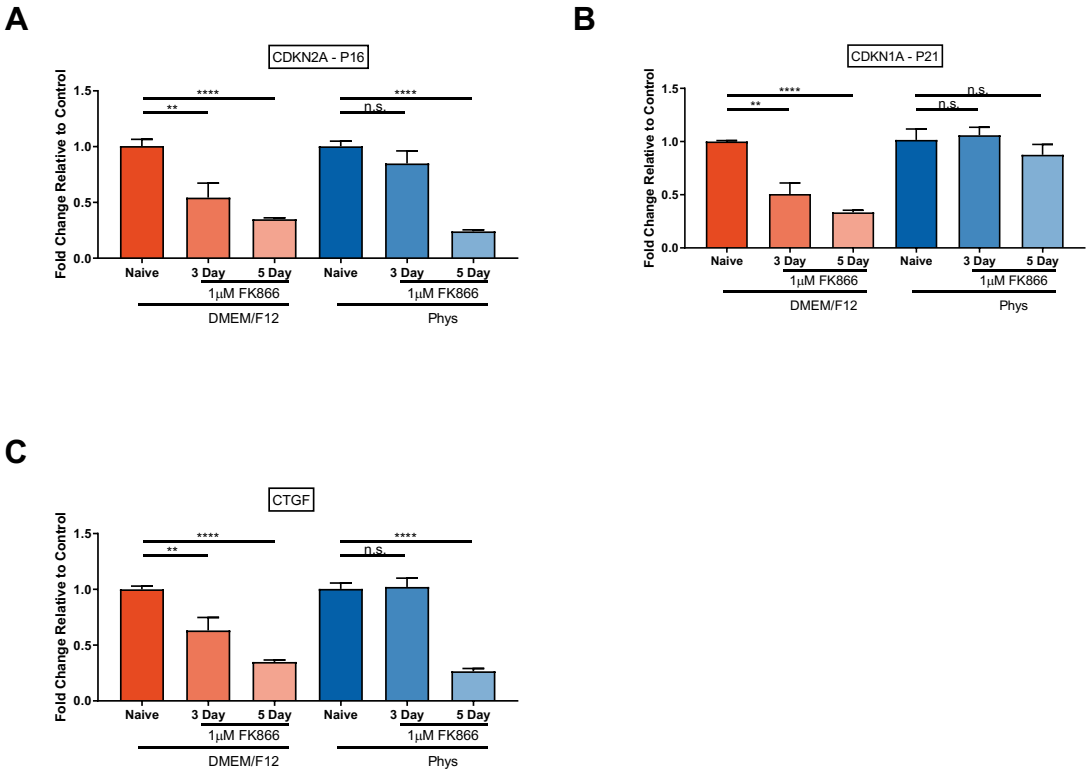

Figure 14. Senescence Markers Decrease with NAMPT Inhibition

Fold change of gene expression relative to the media specific control show some significant decreases in senescence specific genes. CDKN2A, CKDN1A, and CTGF all decrease significantly in a time dependent manner. CDKN1A does not change significantly in the Phys media. Significance was determined by a one-way ordinary ANOVA multiple comparisons test with findings reported as follows; p <0.05 (*), p <0.01 (**), p <0.005 (***), p <0.0001 (****).

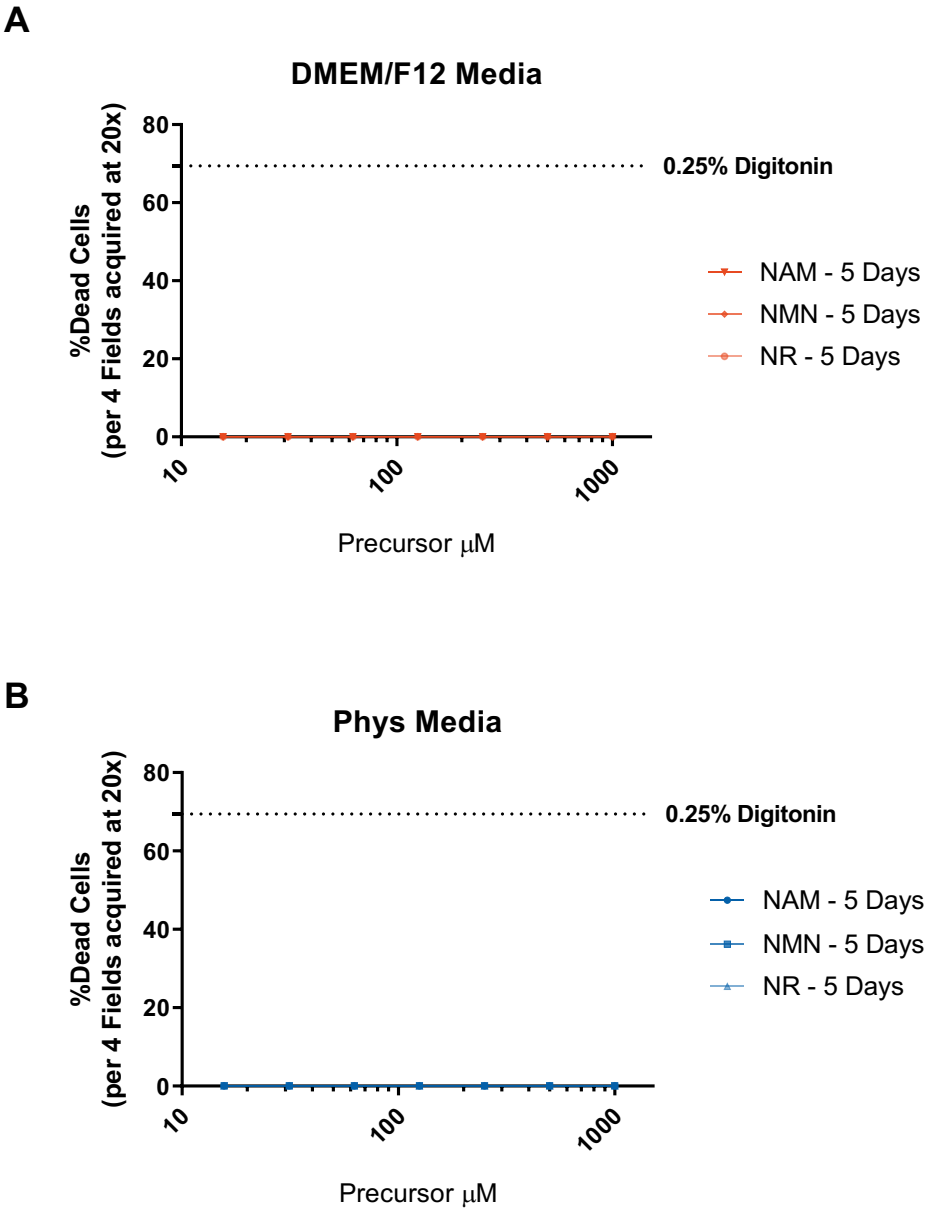

Figure 15. Precursors Alone Did Not Change Live/Dead Cell Stain Readout

Precursors Nicotinamide (NAM), Nicotinamide Mononucleotide (NMN), and Nicotinamide Riboside (NR) did not increase ethidium homodimer-1 signal in any concentrations tested.

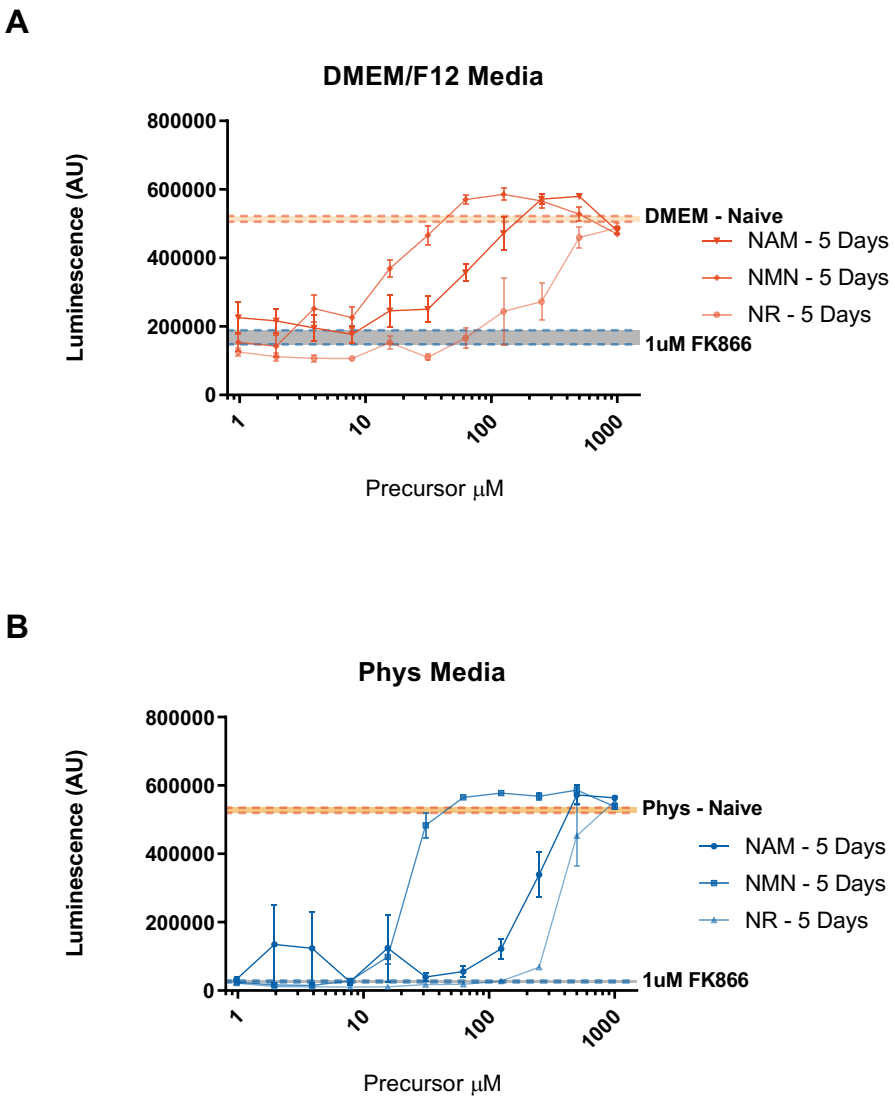

Figure 16. NAD^+ Precursors Do Not reduce Cell Viability

Precursors Nicotinamide (NAM), Nicotinamide Mononucleotide (NMN), and Nicotinamide Riboside (NR), were added at the indicated ranges. In DMEM/F12 NAM and NMN did not affect cell viability except at the highest doses tested (>200μM). Whereas, NMN increased ATP levels in all the tested doses, except 500 and 1000 μM. In Phys media, NR reduced ATP and NM had no affect compared to Phys control. No significant decreases in cell viability were observed in the lower concentrations (N=2). However, NR was able to significantly increase ATP levels by ~13%starting at 31.25μM in DMEM/F12 (p=0.0086, determined by t-test), but not in Phys (p=0.4014).

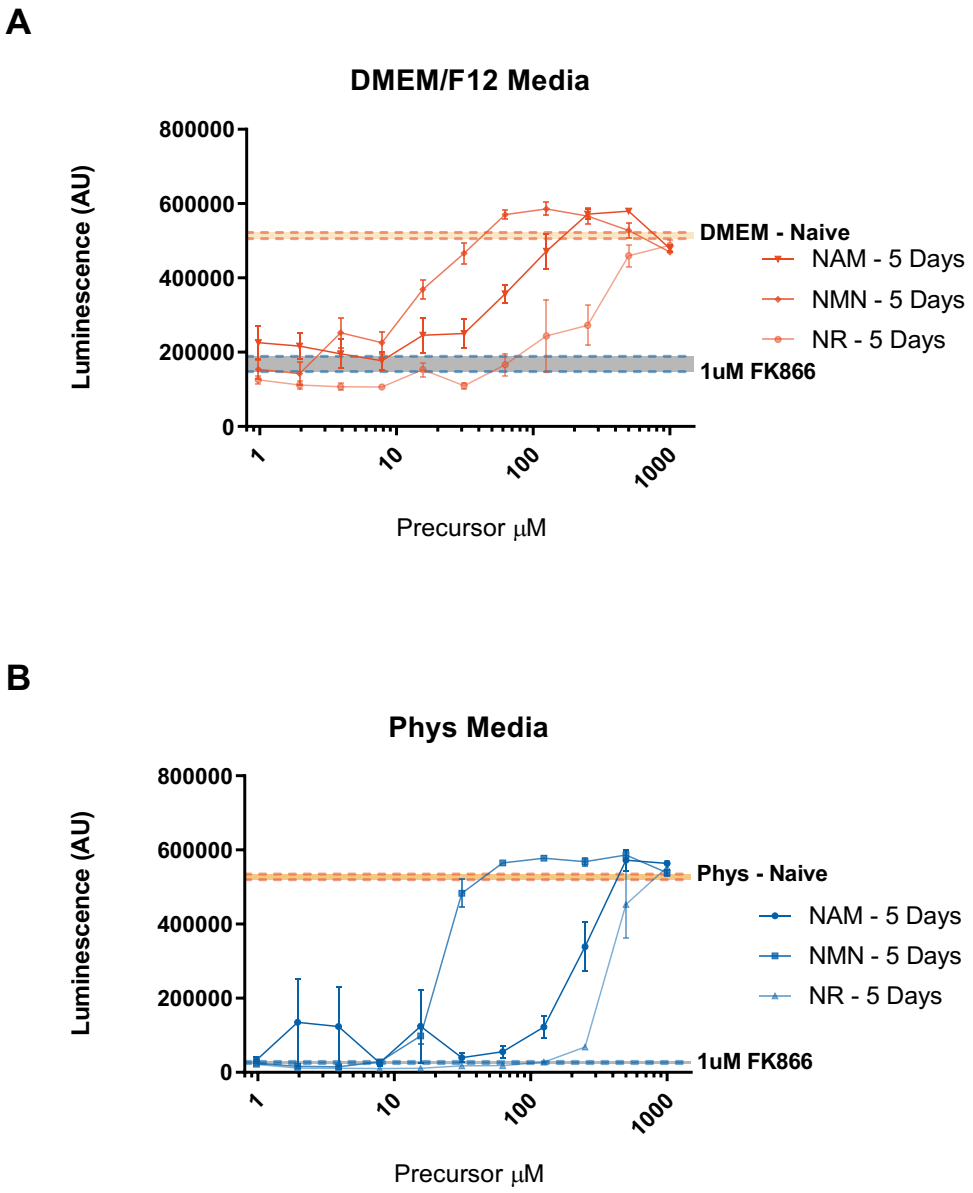

Figure 17. ATP Levels Recover in the Presence of Precursors and a Fixed Dose of FK866

Precursors Nicotinamide (NAM), Nicotinamide Mononucleotide (NMN), and Nicotinamide Riboside (NR) recovered CTG signal at the highest concentrations. NMN exhibited the best profile in both media conditions (n=2). Greater than 50% recovery was observed in the group treated with 31.25μM of NMN and 1μM FK866 in both DMEM/F12 (p=0.0382, when compared to Naive) and Phys media (p=0.0901, when compared to naive).

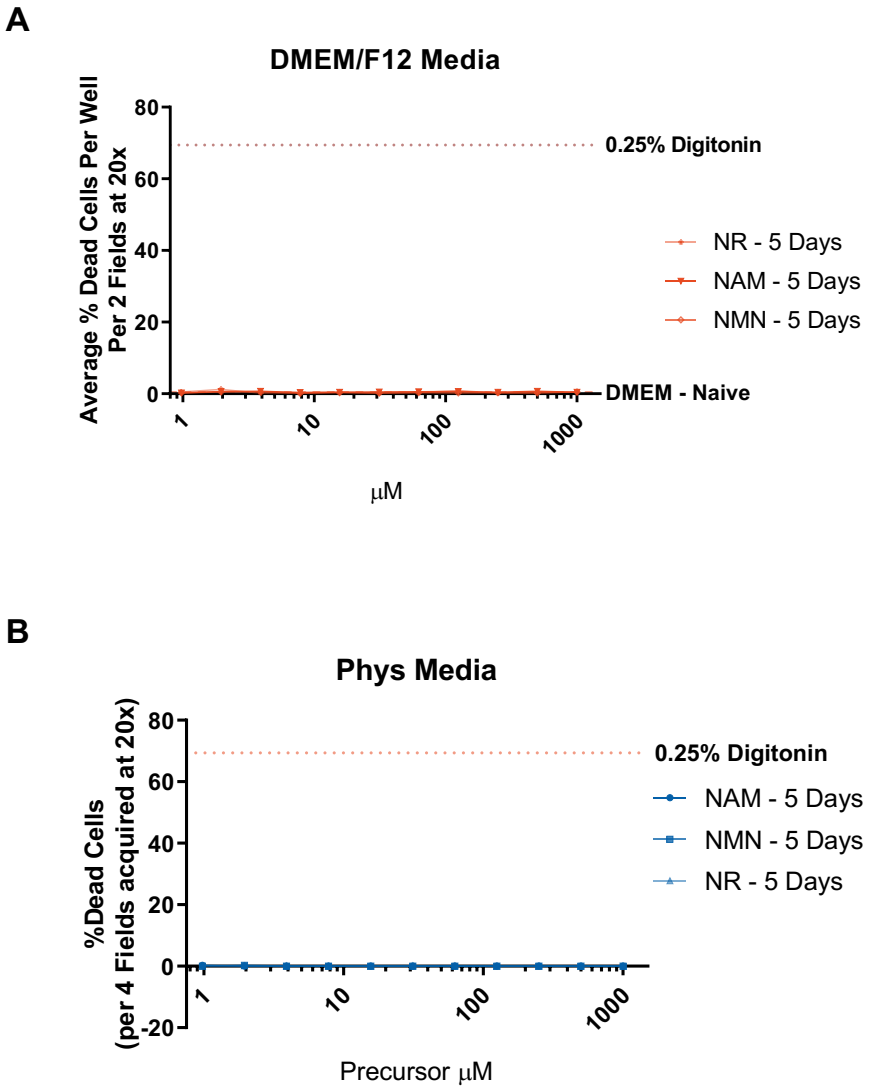

Figure 17. Live/Dead Cell Stain was Not Affected by Precursors with Fixed Dose of FK866

A response from 1mM to 1μM of precursors Nicotinamide (NAM), Nicotinamide Mononucleotide (NMN), and Nicotinamide Riboside (NR) did not increase cell death significantly at any concentration. Only one dose response showed signs of increasing cell death with decreasing precursor concentrations (N=3).

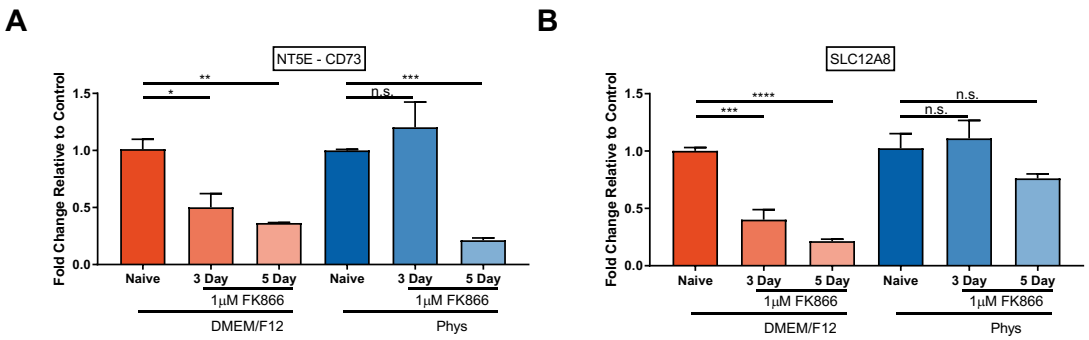

Figure 18. Precursors Transporters are Changed by NAD^+/NADH Depletion in ARPE-19 Cells

Gene expression of NR or NMN transporters showed a decrease in expression after treatment with FK866. In DMEM/F12 expression of NT5E (A) decreased significantly at 3 and 5 days of treatment (p=0.016, and 0.0022 respectively). Phys showed a significant reduction at 5 days (A, p=0.0003). Interestingly SLC12A8 (B) did not have a significant reduction in expression in Phys media, but did in DMEM/F12 (p=0.0009, and, 0.0001 respectively). Significance was determined by a one-way ordinary ANOVA multiple comparisons test with findings reported as follows; p <0.05 (*), p <0.01 (**), p <0.005 (***), p <0.0001 (****).

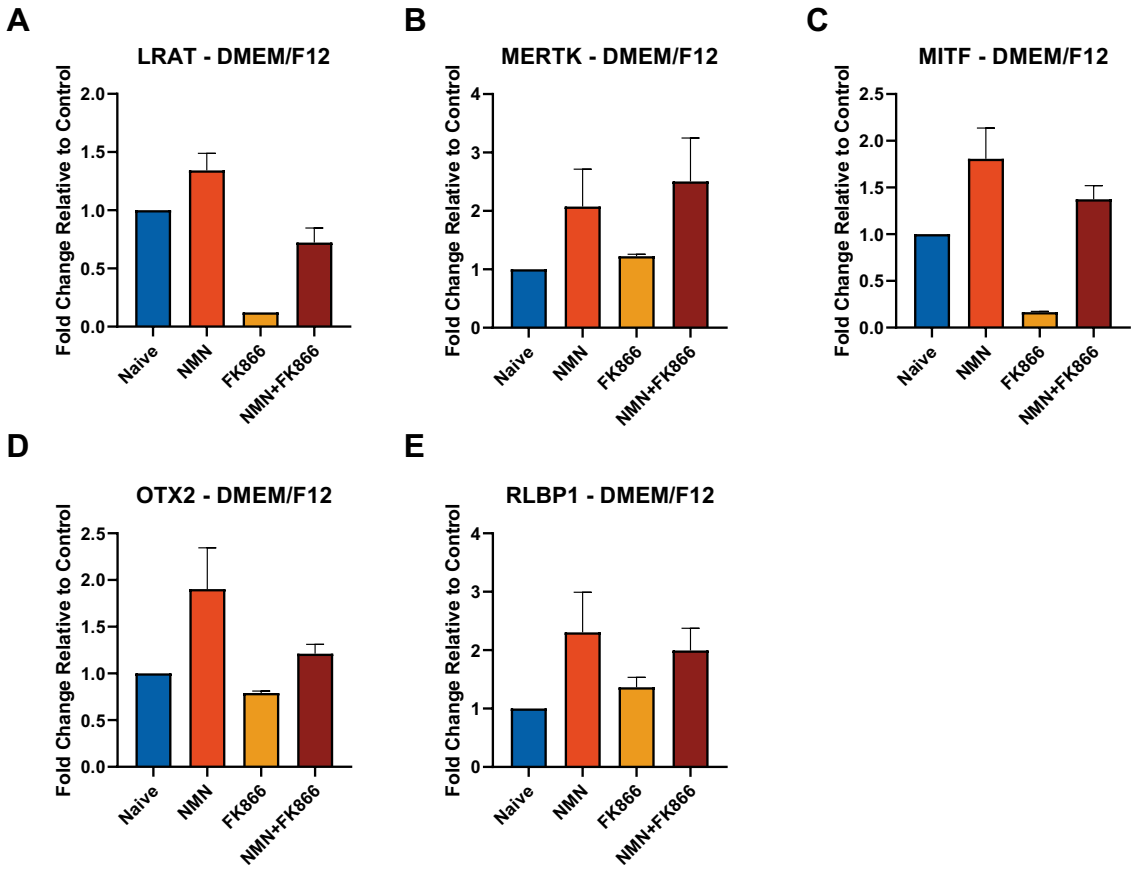

Figure 19. RPE Markers Recover with NMN in Cells Treated with FK866 for 5 Days in DMEM/F12

ARPE-19 cells treated with 1μM FK866 for 5 days had decreased gene expression for only two of the five markers tested, LRAT, and MERTK. This phenotype could be reversed with the additional treatment of 20μM NMN for 5 days. NMN treatment alone also increased the expression of all RPE markers we tested, but only in DMEM/F12.

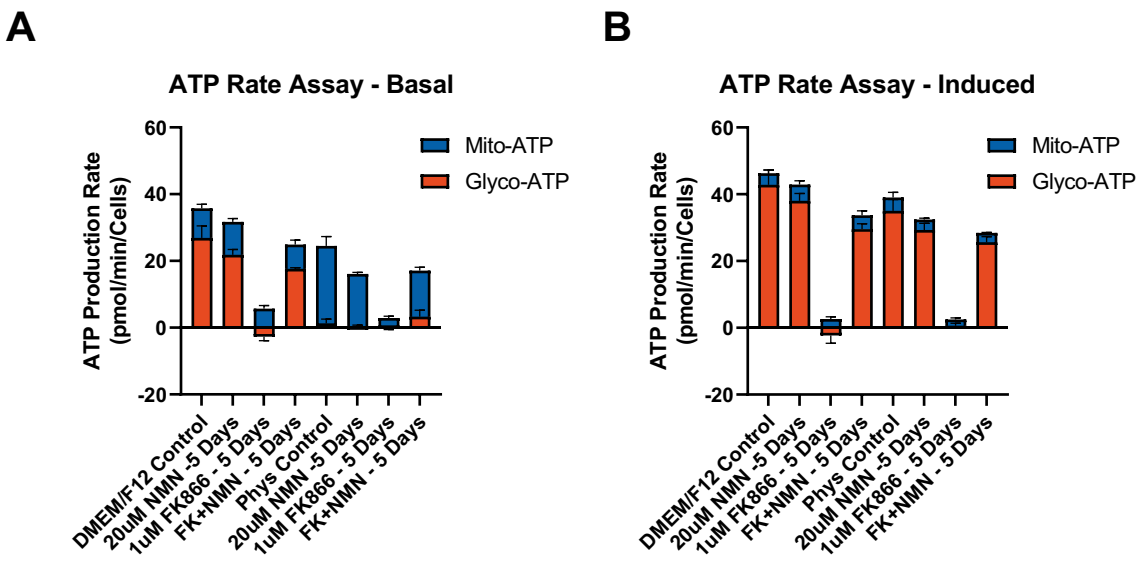

Figure 20. ATP Rate Assay of NMN Rescues the Metabolic Profile of ARPE-19 cells

Treated with FK866

NMN treatment alone did not significantly affect the metabolism of ARPE-19 cells in either media conditions. NMN in combination with FK866 were able to recover their ATP production rates and maintained similar fractions of mitochondrial to glycolysis (n=2). Basal Mitochondrial ATP production was not significantly changed in any treatment condition in the DMEM/F12 media ($p>0.9999$ for all comparisons). However, basal Mitochondrial ATP production rate was significantly reduced in cells treated with FK866, and the combination treatments when compared to the untreated control ($p<0.0001$ for both conditions). Both induced Mitochondrial and Glycolysis ATP production rates were not significantly changed by the addition of NMN in either media condition ($p>0.9999$). Glycolysis ATP production was significantly reduced in cells treated with FK866 in both media types ($p<0.0001$ respectively). Combination treatments of FK866 and NMN significantly reduced glycolysis ATP production rate but were less significant ($p=0.0081$ in DMEM/F12, $p=0.0004$). Significance was determined using a three-way anova with a Bonferroni's multiple comparisons test.

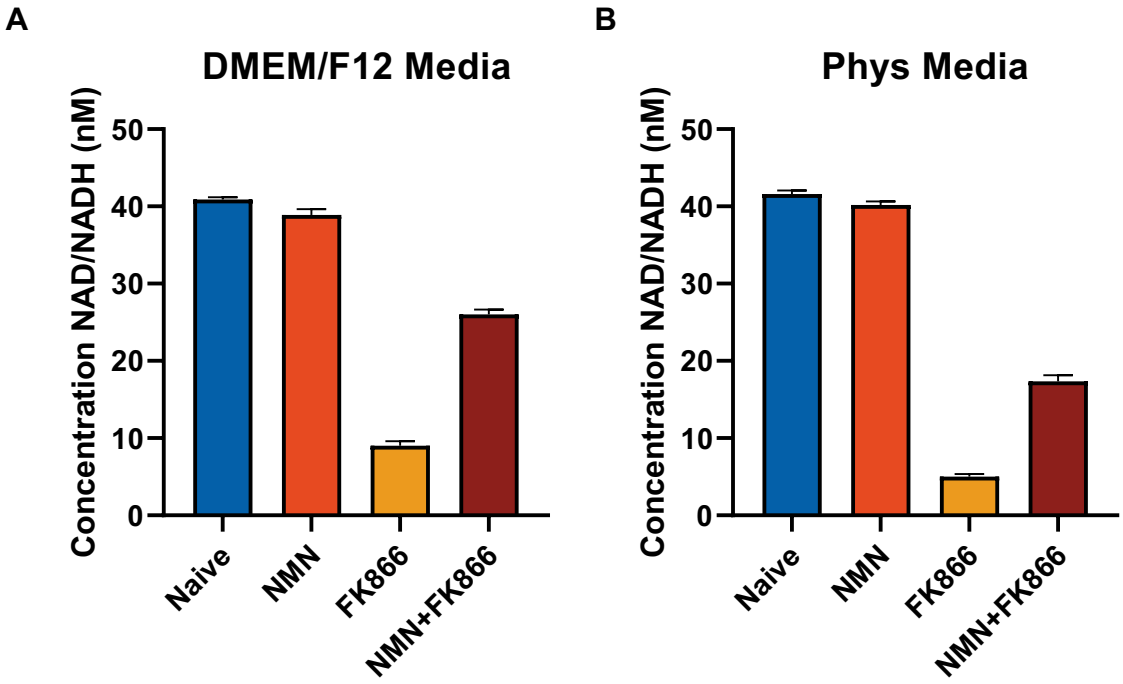

Figure 21. NMN Partially Rescues NAD^+/NADH in ARPE19 Treated challenged with NAMPT Inhibition

A 20μM Nicotinamide Mononucleotide (NMN) alone was not able to increase the concentration of intracellular NAD^+/NADH above control concentrations, while FK866 alone (1 μM) was able to reduce the concentration significantly ($p<0.0001$ in both conditions). Combination treatment of FK866 and NMN at the doses described recovered of NAD^+/NADH concentrations in both media (N=3, $p<0.0001$). DMEM/F12 showed a higher recovery, 64%, whereas Phys had slightly less recovery, 42%. Significance was determined by a one-way ordinary ANOVA multiple comparisons test with findings reported as follows; $p<0.05$ (*), $p<0.01$ (**), $p<0.005$ (***), $p<0.0001$ (****).

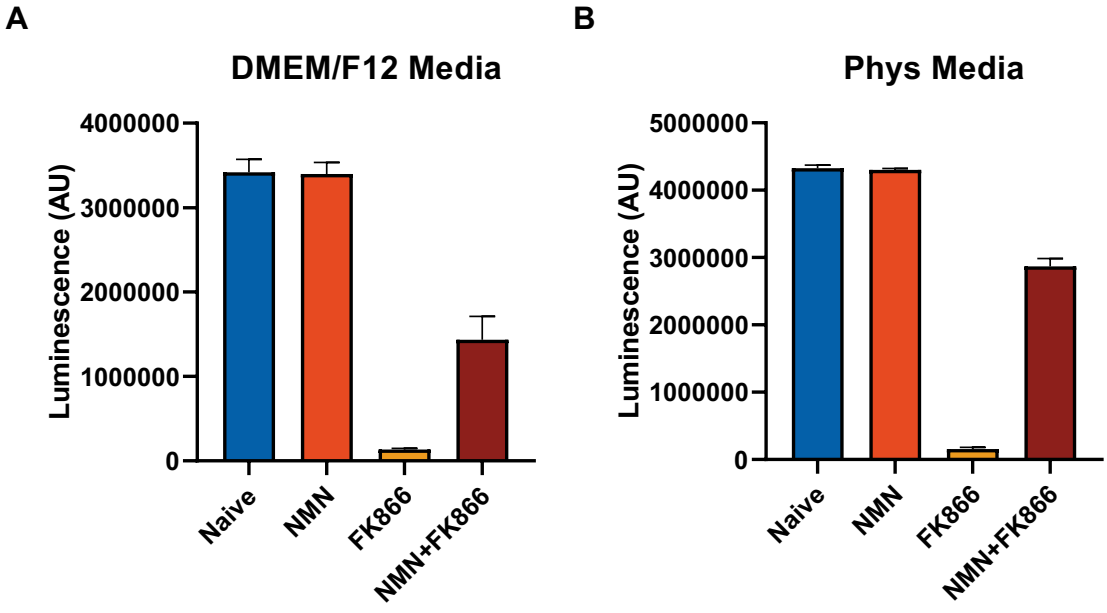

Figure 22. The NAD^+ Precursor NMN Partially Rescues ATP Levels in ARPE-19 challenged with NAMPT Inhibition

A 20μM Nicotinamide Mononucleotide (NMN) alone was not able to increase the concentration of intracellular ATP above control concentrations, while FK866 alone was able to reduce the concentration significantly. Combination treatments of FK866 and NMN showed recovery of intracellular ATP.

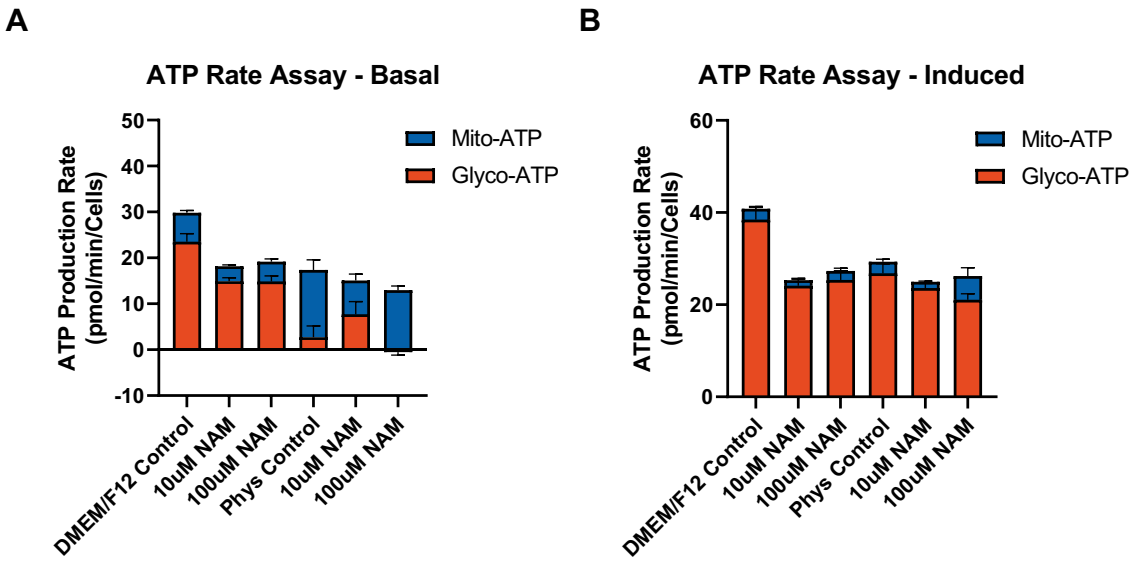

Figure 23. Extracellular NAM Supplementation Inhibits Metabolic Profile of ARPE-19 Cells

NAM supplementation with either 10 or 100μM significantly reduced the glycolytic ATP production in the ARPE-19 cells treated DMEM/F12. 100μM NAM abolished glycolysis in ARPE-19 cells in the Phys media (n=1).

References

Avalos, J. L., Bever, K. M., & Wolberger, C. (2005). Mechanism of sirtuin inhibition by nicotinamide: altering the NAD(+) cosubstrate specificity of a Sir2 enzyme. *Mol Cell, 17*(6), 855-868. doi:10.1016/j.molcel.2005.02.022

Balaratnasingam, C., Yannuzzi, L. A., Curcio, C. A., Morgan, W. H., Querques, G., Capuano, V., . . . Freund, K. B. (2016). Associations Between Retinal Pigment Epithelium and Drusen Volume Changes During the Lifecycle of Large Drusenoid Pigment Epithelial Detachments. *Invest Ophthalmol Vis Sci, 57*(13), 5479-5489. doi:10.1167/iovs.16-19816

Cantor, J. R., Abu-Remaileh, M., Kanarek, N., Freinkman, E., Gao, X., Louissaint, A., Jr., . . . Sabatini, D. M. (2017). Physiologic Medium Rewires Cellular Metabolism and Reveals Uric Acid as an Endogenous Inhibitor of UMP Synthase. *Cell, 169*(2), 258-272 e217. doi:10.1016/j.cell.2017.03.023

Chen, Z., Zhai, Y., Zhang, W., Teng, Y., & Yao, K. (2015). Single Nucleotide Polymorphisms of the Sirtuin 1 (SIRT1) Gene are Associated With age-Related Macular Degeneration in Chinese Han Individuals: A Case-Control Pilot Study. *Medicine (Baltimore), 94*(49), e2238. doi:10.1097/MD.0000000000002238

Chiang, P. W., Wang, J., Chen, Y., Fu, Q., Zhong, J., Chen, Y., . . . Qi, M. (2012). Exome sequencing identifies NMNAT1 mutations as a cause of Leber congenital amaurosis. *Nat Genet, 44*(9), 972-974. doi:10.1038/ng.2370

Curcio, C. A. (2018). Soft Drusen in Age-Related Macular Degeneration: Biology and Targeting Via the Oil Spill Strategies. *Invest Ophthalmol Vis Sci, 59*(4), AMD160-AMD181. doi:10.1167/iovs.18-24882

Du, J., Yanagida, A., Knight, K., Engel, A. L., Vo, A. H., Jankowski, C., . . . Chao, J. R. (2016). Reductive carboxylation is a major metabolic pathway in the retinal pigment epithelium. *Proc Natl Acad Sci U S A, 113*(51), 14710-14715. doi:10.1073/pnas.1604572113

Fang, E. F., Lautrup, S., Hou, Y., Demarest, T. G., Croteau, D. L., Mattson, M. P., & Bohr, V. A. (2017). NAD(+) in Aging: Molecular Mechanisms and Translational Implications. *Trends Mol Med, 23*(10), 899-916. doi:10.1016/j.molmed.2017.08.001

Fasler-Kan, E., Aliu, N., Wunderlich, K., Ketterer, S., Ruggiero, S., Berger, S., & Meyer, P. (2018). The Retinal Pigment Epithelial Cell Line (ARPE-19) Displays Mosaic Structural Chromosomal Aberrations. *Methods Mol Biol, 1745*, 305-314. doi:10.1007/978-1-4939-7680-5_17

Feher, J., Kovacs, I., Artico, M., Cavallotti, C., Papale, A., & Balacco Gabrieli, C. (2006). Mitochondrial alterations of retinal pigment epithelium in age-related

macular degeneration. *Neurobiol Aging, 27*(7), 983-993. doi:10.1016/j.neurobiolaging.2005.05.012

Fouquerel, E., Goellner, E. M., Yu, Z., Gagne, J. P., Barbi de Moura, M., Feinstein, T., . . . Sobol, R. W. (2014). ARTD1/PARP1 negatively regulates glycolysis by inhibiting hexokinase 1 independent of NAD+ depletion. *Cell Rep, 8*(6), 1819-1831. doi:10.1016/j.celrep.2014.08.036

Garten, A., Schuster, S., Penke, M., Gorski, T., de Giorgis, T., & Kiess, W. (2015). Physiological and pathophysiological roles of NAMPT and NAD metabolism. *Nat Rev Endocrinol, 11*(9), 535-546. doi:10.1038/nrendo.2015.117

Gaur, U., Tu, J., Li, D., Gao, Y., Lian, T., Sun, B., . . . Yang, M. (2017). Molecular evolutionary patterns of NAD+/Sirtuin aging signaling pathway across taxa. *PLoS One, 12*(8), e0182306. doi:10.1371/journal.pone.0182306

Golestaneh, N., Chu, Y., Cheng, S. K., Cao, H., Poliakov, E., & Berinstein, D. M. (2016). Repressed SIRT1/PGC-1alpha pathway and mitochondrial disintegration in iPSC-derived RPE disease model of age-related macular degeneration. *J Transl Med, 14*(1), 344. doi:10.1186/s12967-016-1101-8

Gong, B., Pan, Y., Vempati, P., Zhao, W., Knable, L., Ho, L., . . . Pasinetti, G. M. (2013). Nicotinamide riboside restores cognition through an upregulation of proliferator-activated receptor-gamma coactivator 1alpha regulated beta-secretase 1 degradation and mitochondrial gene expression in Alzheimer's mouse models. *Neurobiol Aging, 34*(6), 1581-1588. doi:10.1016/j.neurobiolaging.2012.12.005

Goody, M. F., & Henry, C. A. (2018). A need for NAD+ in muscle development, homeostasis, and aging. *Skelet Muscle, 8*(1), 9. doi:10.1186/s13395-018-0154-1

Grozio, A., Mills, K. F., Yoshino, J., Bruzzone, S., Sociali, G., Tokizane, K., . . . Imai, S. I. (2019). Slc12a8 is a nicotinamide mononucleotide transporter. *Nat Metab, 1*(1), 47-57. doi:10.1038/s42255-018-0009-4

Guan, X., Lin, P., Knoll, E., & Chakrabarti, R. (2014). Mechanism of inhibition of the human sirtuin enzyme SIRT3 by nicotinamide: computational and experimental studies. *PLoS One, 9*(9), e107729. doi:10.1371/journal.pone.0107729

Guntur, A. R., Gerencser, A. A., Le, P. T., DeMambro, V. E., Bornstein, S. A., Mookerjee, S. A., . . . Rosen, C. J. (2018). Osteoblast-like MC3T3-E1 Cells Prefer Glycolysis for ATP Production but Adipocyte-like 3T3-L1 Cells Prefer Oxidative Phosphorylation. *J Bone Miner Res, 33*(6), 1052-1065. doi:10.1002/jbmr.3390

Hou, Y., Lautrup, S., Cordonnier, S., Wang, Y., Croteau, D. L., Zavala, E., . . . Bohr, V. A. (2018). NAD(+) supplementation normalizes key Alzheimer's features and DNA damage responses in a new AD mouse model with introduced DNA repair deficiency. *Proc Natl Acad Sci U S A, 115*(8), E1876-E1885. doi:10.1073/pnas.1718819115

Houtkooper, R. H., Canto, C., Wanders, R. J., & Auwerx, J. (2010). The secret life of NAD+: an old metabolite controlling new metabolic signaling pathways. *Endocr Rev, 31*(2), 194-223. doi:10.1210/er.2009-0026

Imai, S., & Guarente, L. (2014). NAD+ and sirtuins in aging and disease. *Trends Cell Biol, 24*(8), 464-471. doi:10.1016/j.tcb.2014.04.002

Jadeja, R. N., Powell, F. L., Jones, M. A., Fuller, J., Joseph, E., Thounaojam, M. C., . . . Martin, P. M. (2018). Loss of NAMPT in aging retinal pigment epithelium reduces NAD(+) availability and promotes cellular senescence. *Aging (Albany NY), 10*(6), 1306-1323. doi:10.18632/aging.101469

Jager, R. D., Mieler, W. F., & Miller, J. W. (2008). Age-related macular degeneration. *N Engl J Med, 358*(24), 2606-2617. doi:10.1056/NEJMra0801537

Jarrett, S. G., & Boulton, M. E. (2007). Poly(ADP-ribose) polymerase offers protection against oxidative and alkylation damage to the nuclear and mitochondrial genomes of the retinal pigment epithelium. *Ophthalmic Res, 39*(4), 213-223. doi:10.1159/000104683

Johnson, S., & Imai, S. I. (2018). NAD (+) biosynthesis, aging, and disease. *F1000Res, 7*, 132. doi:10.12688/f1000research.12120.1

Kauppinen, A., Paterno, J. J., Blasiak, J., Salminen, A., & Kaarniranta, K. (2016). Inflammation and its role in age-related macular degeneration. *Cell Mol Life Sci, 73*(9), 1765-1786. doi:10.1007/s00018-016-2147-8

Kevany, B. M., & Palczewski, K. (2010). Phagocytosis of retinal rod and cone photoreceptors. *Physiology (Bethesda), 25*(1), 8-15. doi:10.1152/physiol.00038.2009

Lim, L. S., Mitchell, P., Seddon, J. M., Holz, F. G., & Wong, T. Y. (2012). Age-related macular degeneration. *Lancet, 379*(9827), 1728-1738. doi:10.1016/S0140-6736(12)60282-7

Lin, J. B., Kubota, S., Ban, N., Yoshida, M., Santeford, A., Sene, A., . . . Apte, R. S. (2016). NAMPT-Mediated NAD(+) Biosynthesis Is Essential for Vision In Mice. *Cell Rep, 17*(1), 69-85. doi:10.1016/j.celrep.2016.08.073

Liu, L. Y., Wang, F., Zhang, X. Y., Huang, P., Lu, Y. B., Wei, E. Q., & Zhang, W. P. (2012). Nicotinamide phosphoribosyltransferase may be involved in age-related brain diseases. *PLoS One, 7*(10), e44933. doi:10.1371/journal.pone.0044933

Massudi, H., Grant, R., Braidy, N., Guest, J., Farnsworth, B., & Guillemin, G. J. (2012). Age-associated changes in oxidative stress and NAD+ metabolism in human tissue. *PLoS One, 7*(7), e42357. doi:10.1371/journal.pone.0042357

Mookerjee, S. A., Gerencser, A. A., Nicholls, D. G., & Brand, M. D. (2018). Quantifying intracellular rates of glycolytic and oxidative ATP production and consumption using extracellular flux measurements. *J Biol Chem, 293*(32), 12649-12652. doi:10.1074/jbc.AAC118.004855

Moon, P., & Minhas, P. (2017). Teasing apart NAD(+) metabolism in inflammation: commentary on Zhou et al. (2016). Br J Pharmacol 173: 2352-2368. *Br J Pharmacol, 174*(3), 281-283. doi:10.1111/bph.13677

Okabe, K., Yaku, K., Tobe, K., & Nakagawa, T. (2019). Implications of altered NAD metabolism in metabolic disorders. *J Biomed Sci, 26*(1), 34. doi:10.1186/s12929-019-0527-8

Prasad, P. S., Schwartz, S. D., & Hubschman, J. P. (2010). Age-related macular degeneration: current and novel therapies. *Maturitas, 66*(1), 46-50. doi:10.1016/j.maturitas.2010.02.006

Schutt, F., Aretz, S., Auffarth, G. U., & Kopitz, J. (2012). Moderately reduced ATP levels promote oxidative stress and debilitate autophagic and phagocytic capacities in human RPE cells. *Invest Ophthalmol Vis Sci, 53*(9), 5354-5361. doi:10.1167/iovs.12-9845

Srivastava, S. (2016). Emerging therapeutic roles for NAD(+) metabolism in mitochondrial and age-related disorders. *Clin Transl Med, 5*(1), 25. doi:10.1186/s40169-016-0104-7

Toops, K. A., Tan, L. X., & Lakkaraju, A. (2014). A detailed three-step protocol for live imaging of intracellular traffic in polarized primary porcine RPE monolayers. *Exp Eye Res, 124*, 74-85. doi:10.1016/j.exer.2014.05.003

Zabka, T. S., Singh, J., Dhawan, P., Liederer, B. M., Oeh, J., Kauss, M. A., . . . Misner, D. L. (2015). Retinal toxicity, in vivo and in vitro, associated with inhibition of nicotinamide phosphoribosyltransferase. *Toxicol Sci, 144*(1), 163-172. doi:10.1093/toxsci/kfu268

Zhao, C., Yasumura, D., Li, X., Matthes, M., Lloyd, M., Nielsen, G., . . . Vollrath, D. (2011). mTOR-mediated dedifferentiation of the retinal pigment epithelium initiates photoreceptor degeneration in mice. *J Clin Invest, 121*(1), 369-383. doi:10.1172/JCI44303

Zhou, M., Luo, J., & Zhang, H. (2018). Role of Sirtuin 1 in the pathogenesis of ocular disease (Review). *Int J Mol Med, 42*(1), 13-20. doi:10.3892/ijmm.2018.3623

Zhu, X. H., Lu, M., Lee, B. Y., Ugurbil, K., & Chen, W. (2015). In vivo NAD assay reveals the intracellular NAD contents and redox state in healthy human brain and their age dependences. *Proc Natl Acad Sci U S A, 112*(9), 2876-2881. doi:10.1073/pnas.1417921112